

Galaxy groups and clouds in the Local ($z \sim 0.01$) universe

Dmitry Makarov^{1,2,3*}, Igor Karachentsev^{1,2}

¹*Special Astrophysical Observatory, Nizhniy Arkhyz, Karachai-Cherkessia 369167, Russia*

²*Université de Lyon, Université Lyon 1, CNRS/IN2P3, Institut de Physique Nucléaire de Lyon, Villeurbanne, France*

³*Isaac Newton Institute of Chile, SAO Branch, Russia*

Accepted 2010 November 23. Received 2010 November 23; in original form 2010 August 01

ABSTRACT

We present an all-sky catalogue of 395 nearby galaxy groups revealed in the Local Supercluster and its surroundings. The groups and their associations are identified among 10914 galaxies at $|b| > 15^\circ$ with radial velocities $V_{LG} < 3500 \text{ km s}^{-1}$. Our group finding algorithm requires the group members to be located inside their zero-velocity surface. Hereby, we assume that individual galaxy masses are proportional to their total K -band luminosities, $M/L_K = 6 M_\odot/L_\odot$.

The sample of our groups, where each group has $n \geq 4$ members, is characterized by the following medians: mean projected radius $\langle R \rangle = 268 \text{ kpc}$, radial velocity dispersion $\sigma_V = 74 \text{ km s}^{-1}$, K -band luminosity $L_K = 1.2 \cdot 10^{11} L_\odot$, virial and projected masses $M_{vir} = 2.4 \cdot 10^{12}$ and $M_p = 3.3 \cdot 10^{12} M_\odot$, respectively. Accounting for measurement error reduces the median masses by 30 per cent. For 97 per cent of identified groups the crossing time does not exceed the cosmic time, 13.7 Gyr, having the median at 3.8 Gyr.

We examine different properties of the groups, in particular, of the known nearby groups and clusters in Virgo and Fornax. About a quarter of our groups can be classified as fossil groups where the dominant galaxy is at least ten times brighter than the other group members.

In total, our algorithm identifies 54 per cent of galaxies to be members of groups. Together with triple systems and pairs they gather 82 per cent of the K -band light in Local universe. We have obtained the local value of matter density to be $\Omega_m = 0.08 \pm 0.02$ within a distance of $\sim 40 \text{ Mpc}$ assuming $H_0 = 73 \text{ km s}^{-1} \text{ Mpc}^{-1}$. It is significantly smaller than the cosmic value, 0.28, in the standard Λ CDM model. The discrepancy between the global and local quantities of Ω_m may be caused by the existence of Dark Matter component unrelated to the virial masses of galaxy systems.

Key words: catalogues – galaxies: groups: general – cosmological parameters

1 INTRODUCTION

As the observational data show, the bulk of galaxies inhabit the groups with a number of members from two to a hundred or more. Our Galaxy and its companions are no exception, forming a group with the population $n \sim 25$. The main features of the Local Group and other closest (and therefore the most studied) groups were examined by Karachentsev (2005). Due to their abundance, the groups of galaxies make a main contribution to the average density of matter in the universe. However, according to Karachentsev (2005), this contribution in the Local Volume with the radius of 10 Mpc around us amounts to just $\Omega_{m,loc} \sim 0.1$ in the units of critical density, what is significantly lower than the global cosmic value $\Omega_m \sim 0.28$ (Fukugita & Peebles 2004; Spergel et al.

2007) with the Hubble constant $H_0 = 73 \text{ km s}^{-1} \text{ Mpc}^{-1}$. Such a difference may be due to the smallness of the Local Volume, where the statistics of groups is insufficient or does not cover all the variety of groups according to their morphological population and structure. Therefore it is essential to determine the mean local density of matter in larger volume where statistical fluctuations do not introduce significant uncertainty. Despite of 15 per cent variance of density on scale of 80 Mpc (Pápai & Szapudi 2010), this volume is big enough to be considered as fair approximation to mean properties of the Universe.

New mass surveys of galaxy redshifts: 2dF (Colless et al. 2001), HIPASS (Barnes et al. 2001), 6dF (Jones et al. 2004), ALFALFA (Giovannelli et al. 2005), SDSS (Abazajian et al. 2009) present extensive opportunities for finding the groups of galaxies with a particular algorithm. However, the surveys of the sky in the selected regions up to high redshifts $z > 0.1$

* E-mail: dim@sao.ru

appear to be insufficient for the analysis of small-scale clustering due to the loss of a great number of low-luminosity dwarf galaxies in the distant volumes. For example, in the Sloan Digital Sky Survey (SDSS), covering a quarter of the sky, the average distance between the galaxies with measured radial velocities is 9 Mpc, what is an order of magnitude larger than the diameter of a typical galaxy group. For a comparison, note that in the well-studied Local Volume the density of galaxies with measured velocities is two orders of magnitude higher than in the SDSS. Therefore, a sensible strategy in the study of galaxy groups would be to create a representative catalogue of nearby systems over the entire sky within the radius $z \sim 0.01$.

Successful attempts to create a catalogue of nearby groups were made by Vennik (1984, 1987); Tully (1987, 1988); Magtesyan (1988), who used the method of a ‘hierarchical tree’ proposed by Materne (1978, 1979). Tully’s catalogue and atlas of galaxy groups has 179 pairs and groups, selected among 2367 galaxies with the radial velocities of less than 3000 km s^{-1} . About 2/3 of the 2367 galaxies in the above catalogue appeared to be the members of multiple systems. Based on the virial mass estimates for these groups, Tully determined the lower limit of the mean density in the studied volume as $\Omega_{m,loc} \simeq 0.08$. Similar estimates, $\Omega_{m,loc} \sim 0.08$ and 0.05 , were obtained by Vennik (1987) and Magtesyan (1988), respectively. However, other authors, Huchra & Geller (1982); Maia et al. (1989), who used the percolation method (the so-called ‘friend of friend’ method) to isolate the groups, obtained 3–5 times higher estimates of Ω_m .

Over the past 20 years the number of galaxies in the volume of the Local Supercluster and its environs with radial velocities relative to the centroid of the Local Group $V_{LG} < 3500 \text{ km s}^{-1}$ has grown by more than 4 times. The updates of the observational database on the radial velocities, and appearance of a homogeneous across the sky 2MASS near-infrared photometric survey (Jarrett et al. 2003, 2000) enables us to study the structure and kinematics of nearby galaxy groups with significantly greater detail.

This work is a continuation of a series of papers addressing the properties of binary (Karachentsev & Makarov 2008) and triple (Makarov & Karachentsev 2009) systems of galaxies, detected with one and the same algorithm, applied to the same set of the observational data. These catalogues contain, respectively, 509 binary systems and 168 triplets of galaxies. In addition to these, we have compiled a catalogue of 513 isolated galaxies, which are the most isolated objects in the studied volume $V_{LG} < 3500 \text{ km s}^{-1}$ (Karachentsev et al. 2009). In this paper we present a catalogue of 395 multiple systems with the populations of four or more members, and discuss the basic properties of these groups.

2 OBSERVATIONAL DATA

We use the HyperLEDA¹ (Paturel et al. 2003) and the NED² databases as main sources of data on radial velocities, apparent magnitudes, morphological types and other parameters

of galaxies. It must be emphasized that their use requires a critical approach. Both these databases contain a significant amount of ‘spam’. Quite common case is a misidentification of objects due to misprints or imprecise coordinates. Without diminishing the importance of mass surveys like 6dF and others, it is necessary to note they produce significant number of erroneous radial velocities. Apparent magnitudes and radial velocities from the SDSS survey often correspond to individual knots and associations in bright galaxies. It is only tip of the iceberg of different sources of pollution of the databases. We have taken into account and corrected, where possible, these cases, especially significant for selection of tight galaxy systems. As a matter of fact it is most hard and time-consuming part of our work. Because the databases are constantly updated and new invalid data emerge, therefore the error correction is iterative task. Additionally, we made a number of optical identifications of *HI* sources from the HIPASS survey, specifying their coordinates and determining the apparent magnitudes and morphological types of galaxies (Karachentsev et al. 2008). Many dwarf galaxies, especially of low surface brightness, were examined by us on the DSS digital images to determine their main characteristics. A typical error of our visual estimation of a galaxy’s apparent magnitude is $\sim 0.5^m$, and the mean error its type determination is about ± 2 in the digital scale used by de Vaucouleurs et al. (1976) in the RC2 catalogue.

As it is known, the best indicator of stellar mass of a galaxy is its near-infrared luminosity. The stellar mass dominates the baryon mass in most, but not all, galaxies. The near-infrared flux is weakly affected by a dust and young blue star complexes in the galaxy. For this reason, we have taken photometry in *K*-band at $\lambda = 2.16 \mu\text{m}$ as our photometric basis. Most of these data come from the all-sky 2MASS survey (Jarrett et al. 2003, 2000). In case of lack the *K*-band photometry we transferred the optical (*B*, *V*, *R*, *I*) and near-infrared (*J*, *H*) magnitudes of galaxies into the *K*-magnitudes using synthetic colours of galaxies from Buzzoni (2005) and Fukugita et al. (1995). The greatest amount of photometric data for galaxies falls on the *B*-band. Based on the relations between the *B* – *K* colour index and the morphological type, discussed by Jarrett et al. (2003), and Karachentsev & Kutkin (2005), we used the following transformations for the mean colour index:

$$\begin{aligned} \langle B - K \rangle &= +4.10 && \text{for early types, } T \leq 2, \text{ (E, S0, Sa),} \\ \langle B - K \rangle &= +2.35 && \text{where } T \geq 9 \text{ (Sm, Im, Irr),} \\ \langle B - K \rangle &= 4.60 - 0.25T && \text{where } T = 3-8. \end{aligned} \quad (1)$$

Note that owing to short exposures the 2MASS survey turned out to be insensitive to the galaxies with low surface brightness and blue colour. For about a thousand dwarf irregular and spheroidal galaxies, detected recently by Karachentseva & Karachentsev (1998, 2000) in the Local Supercluster volume, there are only eye estimate of *B*-magnitudes, which converted into *K*-magnitudes using the recipe described above. Despite the lack of good photometry for them, gas-rich dIrr galaxies have high-precision radial velocities from the 21-cm line measurements and hence they are important ‘test particles’ to trace the gravitational well of group of galaxies. The need to convert *B*-magnitudes to *K*-band for about 35 per cent of galaxies adds a considerable uncertainty to the mass estimates of that objects, but

¹ <http://leda.univ-lyon1.fr>

² <http://nedwww.ipac.caltech.edu>

because we apply it mainly for dwarf galaxies which are not dominate in the total luminosity this transformation can not change significantly properties of the groups.

We gathered all the available in the HyperLEDA and NED measurements of radial velocities of the galaxies in the Local Supercluster and its neighbourhood. Unreliable and inaccurate measurements, namely, where the velocity measurement error was greater than 75 km s^{-1} , were excluded. In the data of the SDSS, 2dF and 6dF surveys we analysed and removed the measurements with the velocities of $< 600 \text{ km s}^{-1}$, if they were the cases of a Milky Way star projecting onto a distant galaxy. When a galaxy had several measurements of its radial velocity, we chose the median value, and the velocity error was estimated as a variance of all the good measurements.

It is necessary to note that Local Group with all its known members was excluded from calculation because the algorithm does not use information on real distances and uses only radial velocities for clusterization. It makes impossible to estimate the properties of galaxies in the Local Group that introduces a mess with membership in the Local Volume.

Our original sample, cleaned from doubtful cases, contains in total 10914 galaxies with radial velocities in the Local Group rest frame of $V_{LG} < 3500 \text{ km s}^{-1}$, located at the galactic latitudes $|b| > 15^\circ$. For all these galaxies we fixed their apparent magnitudes and morphological types. To avoid influence of the boundaries on properties of groups we also used in our calculations the data on the galaxies located in the boundary regions with $10^\circ < |b| < 15^\circ$ and with $3500 < V_{LG} < 4000 \text{ km s}^{-1}$, as some individual members of groups with large virial velocities could appear there. The sampling of such a depth contains the entire Local Supercluster with its distant outskirts, surrounding voids and ridges of the neighbouring clusters.

3 THE GROUP FINDING ALGORITHM

Various algorithms were proposed to identify the groups of galaxies in samples, limited by apparent magnitudes or galaxy distances. However, they can be reduced to two basic ones: the percolation method ('friend of friend') and the taxonomic method (construction of a hierarchical tree).

Using the percolation technique, Huchra & Geller (1982) combined the galaxies in groups on the condition that their projected mutual linear separations and radial velocity differences were smaller than some threshold values R_c and V_c . At $R_c = 0.52 \text{ Mpc}$ and $V_c = 600 \text{ km s}^{-1}$ they have grouped in the CfA redshift survey about 74 per cent of the galaxies, and obtained the groups with a characteristic radius of $R_h = 1.1 \text{ Mpc}$, radial velocity dispersion $\sigma_V = 208 \text{ km s}^{-1}$, and mean virial mass $\lg(M_{vir}/M_\odot) = 13.5$. This method was applied by many authors to different samples of galaxies. The disadvantage of this method is the arbitrariness of choice of two percolation parameters R_c and V_c , a variation of which strongly affects the characteristic size and mass of groups, as well as the fraction of galaxies belonging to the groups. Tracking some mean contrast of the galaxy number density by the R_c and V_c parameters, the percolation criterion overlooks many real groups in the regions of low density, and finds large non-virialized aggregates in the

regions of overdensity. Another shortcoming of the 'friend of friend' method manifests itself in a strong dependence of the group parameters on the group distance D from the observer. Various attempts to reduce this dependence by introducing the variables $R_c(D)$ and $V_c(D)$ were accompanied by additional arbitrary assumptions. Recently, Crook et al. (2007) applied the percolation method to the 2MASS survey of galaxies, and identified 1710 pairs and 1258 groups of galaxies at the relative density contrast $\delta\rho/\rho = 80$. In this sample, the members of groups and pairs make up, respectively, 36 per cent and 17 per cent. The groups by Crook et al. (2007) with the number of members $n \geq 5$ have a characteristic projection radius of about 1 Mpc, the dispersion of radial velocities of $\sim 200 \text{ km s}^{-1}$ and the mean virial mass $\lg(M_{vir}/M_\odot) \sim 13.5$. Taken the depth of the considered 2MASS sample $D_{max} = 140 \text{ Mpc}$, the contribution of virial masses of these groups in the mean density of matter is $\Omega_m \simeq 0.13$.

Following another, 'taxonomic' method, Vennik (1984); Tully (1988) combined galaxy pairs by the maximum ratio of their luminosity to the cube of mutual distance (L_{ik}/R_{ik}^3) . Then such a pair was replaced by a 'particle' with the total luminosity, and the process of finding a case with $\max(L_{ik}/R_{ik}^3)$ repeated. The process was completed by creation of a single 'hierarchical tree' whose branches united the entire considered sample of galaxies. Clipping the tree branches on some contrast level of the volume luminosity yielded a set of branches-groups, the sizes and virial masses of which were dependent on the selected density (luminosity) contrast. Applying the dendrogram method, both authors obtained a characteristic projection radius of the group of 0.3 Mpc, the mean radial velocity dispersion $\sigma_V \simeq 100 \text{ km s}^{-1}$, and the virial mass to blue luminosity ratio $M_{vir}/L_B \simeq 95 M_\odot/L_\odot$.

The both percolation and dendrogram methods ignore the individual properties of galaxies, considering them as indistinguishable particles. But it is obvious that the same thresholds R_c and V_c may be sufficient for clustering a pair of dwarf galaxies, but they are apparently not sufficient to bind a pair of giant galaxies. This inadequacy of the algorithm leads to a systematic distortion of the virial mass estimates.

Combining the galaxies into the systems of different multiplicity should be done taking into account the individual properties of galaxies. Considering two arbitrary galaxies as a virtual bound pair, we assume (Karachentsev 1994; Makarov & Karachentsev 2000) that the spatial velocity difference V_{12} for the galaxies in a physical pair and their spatial separation R_{12} must satisfy the condition of negative total energy

$$\frac{V_{12}^2 R_{12}}{2GM_{12}} < 1, \quad (2)$$

where M_{12} is the total mass of the pair, and G is the gravitational constant. However, from the observations we only know the velocity difference projected on the line of sight $V_{12,r}$, and the separation projected onto the image plane $R_{12,\perp}$. Two galaxies with a very small difference in radial velocities but a large separation in the sky can satisfy the condition (2) without being mutually bound. Hence the condition of negative total energy of the pair, expressed in terms of the observables

$$\frac{V_{12,r}^2 R_{\perp}}{2GM_{12}} < 1 \quad (3)$$

must be supplemented by another restriction on the maximal distance between the components at their fixed mass M_{12} . The condition when the pair components remain within the sphere of ‘zero-velocity’ (Sandage 1986) takes the form of

$$\frac{\pi H_0^2 R_{\perp}^3}{8GM_{12}} < 1, \quad (4)$$

where H_0 is the Hubble constant.

Our algorithm for galaxy grouping is in fact a variant of the percolation method. Firstly, we select all the pairs satisfying the conditions (3) and (4). Then all the pairs with common main component are combined in a group. If a galaxy turned out to be a companion of several massive galaxies at once, we join it with the most massive neighbour. In a particular case, one group may be a subgroup within a more extended system. In this sense, our algorithm combines the properties of both the ‘friend of friend’ method, and the hierarchical approach. On next stage, we replace the galaxies in the group by fake object with summarized luminosity of all its members and with mean redshift. After that we repeat all the steps from the beginning while some object obeys to bound criteria. Although, the algorithm is based on pairwise criterion on final step the bound condition is determined by the entire group.

We determined the masses of galaxies from their integral luminosity in the near-infrared K_s -band, supposing that they have the same mass-to-luminosity ratio

$$M/L_K = \kappa(M_{\odot}/L_{\odot}), \quad (5)$$

where κ is taken equal to 6. In the fact, the value of $\kappa = 6$ is only more or less arbitrary dimensionless parameter of the algorithm. To bound it we ‘trained’ the clusterization algorithm (3–5) on detailed three-dimensional distribution of galaxies in the Local Volume, where the membership of galaxies in the groups is known from good quality photometric distances. Karachentsev (2005) lists the members of several nearby groups like Cen A and M 81. Unfortunately, as it was noted in previous section, we can not test the algorithm on Local Group, thus we used other nearby groups in the Local Volume. The choice of $\kappa = 6$ is the compromise between a loss of the real members and an impurity of groups by false members. For the $\kappa \leq 4$ we lose significant number of real members while $\kappa \geq 8$ leads to appearance in the groups suspicious members. Moreover, for $\kappa \geq 10$ galaxies are combined into extended non-virialized aggregates. At the given value of $\kappa = 6$ the dwarf companions in the well-known nearby groups are usually located inside the zero velocity surface around the major galaxies of these groups.

4 THE CATALOGUE OF GROUPS

The criteria (3–5) of unifying the galaxies in groups with the parameter $\kappa = 6$ was used for 10914 galaxies with radial velocities $V_{LG} < 3500 \text{ km s}^{-1}$, located outside the Milky Way zone, $|b| > 15^\circ$. This led to an identification of 395 groups with the population of $n \geq 4$ members. In total, these groups

include 4381 galaxies. Together with 1018 components of binary systems (Karachentsev & Makarov 2008) and 504 components of triplets (Makarov & Karachentsev 2009) in the same volume, the total number of clustered galaxies is 5903 or 54 per cent of the total number considered.

The catalogue of galaxy groups as the final result of successive iterations of the use of conditions (3–5) is presented in a short and full version. Table 1 is a compact version of the catalogue, containing the basic group characteristics listed in one row. The full version of the catalogue with the indication of all the individual members of each group is available in the electronic form at <http://www.sao.ru/hq/dim/groups>.

The columns of Table 1 contain the following data:

- 1) principal name of the group’s brightest galaxy, taken, as a rule, from the LEDA;
- 2) equatorial coordinates of the group’s main member at the epoch (J2000.0);
- 3) the number of group members with known radial velocities;
- 4) mean radial velocity of the group in km s^{-1} relative to the centroid of the Local Group;
- 5) the standard deviation of radial velocities of the group members (km s^{-1}) not corrected for the velocity measurement errors;
- 6) mean harmonic radius of the group (kpc); at its computation the distance to the group $\langle D \rangle$ was determined from the mean radial velocity with the Hubble parameter $H_0 = 73 \text{ km s}^{-1} \text{ Mpc}^{-1}$;
- 7) logarithm of the total luminosity of the group in the photometric K_s -band given in the unit of solar luminosity at $M_{\odot,K} = 3.28^m$ (Binney & Merrifield 1998);
- 8) logarithm of the projected mass of the group, as defined by (Heisler et al. 1985, equation 11)

$$M_p = \frac{32}{\pi} \frac{1}{N - 3/2} \sum_{i=1}^N \frac{V_{i,r}^2 R_{i,\perp}}{G} \quad (6)$$

where $V_{i,r}$ and $R_{i,\perp}$ are radial velocity and projected distance of the i th galaxy relative to the centre of the system. It should be noted that this value is statistically biased. To obtain an unbiased mass estimate the square of velocity, $V_{i,r}^2$, has to be corrected for measurement error, $(V_{i,r}^2 - \epsilon^2)$. In case of large errors, ϵ , the unbiased value of the group mass, M_p^c , attains a negative value;

- 9) the projected mass-to-total luminosity ratio in the K -band in solar units;

- 10) morphological type of the group’s main member according to the RC2 classification (de Vaucouleurs et al. 1976);

- 11) difference in apparent K -magnitudes of the first and second members of the group, ranked by K -luminosity;

- 12) group’s membership in an association (cloud, clan), which is identified at a higher value of the dimensionless parameter adopted to be $\kappa = 40$; here the name of the association was given by the name of the group that is dominant in it; as it is evident from these data, a significant number of groups are isolated entities not associated with other neighbouring groups.

Table 1. Main properties of groups.

Group	J2000.0	N	V_{LG}	σ_V	R_h	$\lg L/L_\odot$	$\lg M/M_\odot$	$\lg M/L$	T	Δm_{21}	Association
NGC7814	000314.9+160844	4	1283	34	262	10.98	12.16	1.18	2	5.27	NGC7814
ESO293-034	000619.9-412960	5	1435	59	41	10.18	11.87	1.69	6	3.14	ESO293-034
NGC0055	001453.6-391148	4	111	26	123	9.46	11.37	1.91	9	0.13	NGC0055
NGC0092	002131.7-483729	5	3302	101	40	11.08	12.49	1.41	1	1.16	NGC0092
NGC0134	003022.0-331439	4	1629	121	159	11.29	12.54	1.25	4	3.64	NGC0134
NGC0253	004733.1-251718	6	374	87	275	11.24	12.87	1.63	5	3.66	NGC0253
NGC0289	005242.4-311221	8	1618	81	205	11.01	12.77	1.76	4	0.73	NGC0134
IC0065	010055.4+474055	4	2930	77	142	10.95	12.50	1.55	4	0.71	IC0065
NGC0428	011255.7+005854	4	1289	16	117	10.07	10.96	0.89	9	4.26	NGC0428
NGC0488	012146.9+051524	17	2368	85	200	11.83	13.16	1.33	3	1.03	NGC0488
NGC0524	012447.7+093220	16	2581	147	391	11.79	13.16	1.37	-1	1.67	NGC0488
NGC0584	013120.8-065205	11	1945	63	335	11.63	12.85	1.22	-5	0.67	NGC0584
NGC0628	013641.8+154700	6	831	46	171	10.71	12.18	1.47	5	4.96	NGC0628
NGC0660	014302.4+133842	5	955	29	235	10.64	10.96	0.32	1	4.48	NGC0628
NGC0672	014754.5+272558	5	564	41	74	9.78	11.39	1.61	6	1.78	NGC0672
NGC0681	014910.8-102535	7	1889	140	212	10.94	12.89	1.95	2	0.52	NGC0720
NGC0697	015117.6+222129	10	3080	128	260	11.75	13.17	1.42	5	0.21	NGC0697
NGC0720	015300.5-134419	6	1758	145	352	11.20	13.07	1.87	-5	4.16	NGC0720
NGC0772	015919.6+190027	6	2565	56	258	11.57	12.45	0.88	3	3.08	NGC0772
IC0210	020928.2-094048	8	1975	47	157	10.65	12.27	1.62	4	1.18	IC0210
NGC0864	021527.6+060009	4	1677	25	195	10.65	11.93	1.28	5	3.84	NGC0864
IC1788	021550.0-311204	4	3455	31	512	11.22	11.83	0.61	4	0.25	IC1788
NGC0891	022233.4+422057	18	775	60	197	11.30	12.64	1.34	3	0.30	NGC0891
NGC0908	022304.6-211402	9	1585	60	228	11.18	12.14	0.96	5	3.01	NGC0908
NGC0936	022737.5-010923	12	1592	129	336	11.33	12.95	1.62	-1	1.84	NGC1068
NGC0988	023527.8-092122	22	1437	103	379	11.55	12.98	1.43	6	0.45	NGC1068
NGC1032	023923.7+010538	5	2750	37	429	11.14	12.37	1.23	0	4.06	NGC1068
NGC1068	024240.7-000048	11	1160	80	387	11.54	12.79	1.25	3	1.36	NGC1068
NGC1097	024618.0-301512	4	1189	140	43	11.26	12.53	1.27	3	4.26	NGC1316
NGC1153	025809.6+032133	4	3167	66	311	11.08	12.73	1.65	1	0.31	NGC1153
NGC1187	030237.6-225202	4	1315	48	106	10.60	11.90	1.30	5	4.74	NGC1316
NGC1209	030603.0-153641	6	2597	144	95	11.40	13.13	1.73	-4	0.23	NGC1209
NGC1184	031645.0+804736	4	2489	74	418	11.27	12.80	1.53	2	1.68	NGC1184
NGC1302	031951.2-260338	6	1663	47	383	11.15	12.30	1.15	0	0.55	NGC1316
NGC1299	032009.7-061543	5	2313	49	120	10.41	12.03	1.62	3	1.25	NGC1248
NGC1316	032241.7-371230	111	1411	244	454	12.30	13.94	1.64	-2	0.72	NGC1316
NGC1332	032617.3-212007	22	1469	183	279	11.55	13.39	1.84	-3	0.51	NGC1316
NGC1386	033646.2-355957	8	755	70	165	10.37	12.40	2.03	-1	0.57	NGC1316
NGC1395	033829.8-230140	24	1548	121	378	11.53	13.05	1.52	-5	1.40	NGC1316
NGC1398	033852.1-262016	10	1386	89	612	11.46	13.09	1.63	2	1.13	NGC1316
NGC1407	034011.9-183449	25	1713	167	385	11.61	13.32	1.71	-4	1.96	NGC1316
NGC1433	034201.6-471319	14	946	76	340	11.07	12.84	1.77	1	0.60	NGC1291
NGC1511	035939.8-673820	4	1131	32	77	10.37	11.78	1.41	1	2.25	NGC1553
NGC1512	040354.3-432056	5	714	61	11	10.40	12.02	1.62	1	2.25	NGC1291
NGC1519	040807.6-171134	4	1781	26	238	10.29	11.57	1.28	3	0.56	NGC1316
NGC1532	041204.3-325227	10	1159	89	137	11.25	12.70	1.45	3	1.00	NGC1316
NGC1553	041610.5-554649	29	1022	185	62	11.79	13.56	1.77	-2	0.50	NGC1553
UGC02998	041634.3+024533	5	3317	92	329	11.18	12.90	1.72	3	0.14	NGC1550
NGC1665	044817.1-052539	6	2669	48	380	11.17	12.52	1.35	-2	0.17	NGC1665
NGC1779	050518.1-090850	4	3222	25	536	11.27	11.69	0.42	-0	1.38	NGC1723
NGC1808	050742.3-373047	6	840	118	129	11.04	12.45	1.41	1	0.36	NGC1808
MCG-02-14-003	051107.7-092320	4	2518	56	72	10.50	12.35	1.85	5	0.79	NGC1888
NGC1832	051203.3-154116	6	1839	36	396	10.91	12.09	1.18	4	1.79	NGC1832
NGC1947	052647.6-634536	4	914	30	277	10.56	11.56	1.00	-3	2.86	NGC1553
NGC1964	053321.8-215645	9	1532	83	385	11.07	12.89	1.82	3	1.33	NGC1964
NGC1993	053525.6-174855	4	3029	55	359	10.86	12.14	1.28	-3	3.50	NGC1993
NGC2089	054751.4-173609	5	2818	45	600	11.22	12.49	1.27	-3	0.88	NGC2089
NGC2207	061622.0-212222	5	2570	108	113	11.44	13.07	1.63	4	0.37	NGC2207
ESO489-035	061859.5-243749	4	2557	38	85	10.83	11.37	0.54	-3	0.05	NGC2207
NGC2217	062139.8-271402	5	1559	82	253	11.20	12.41	1.21	-1	2.21	NGC2217
UGC03714	071232.7+714502	4	3074	98	235	11.09	12.86	1.77	5	0.18	UGC03714
ESO162-017	071554.5-572037	4	837	32	97	9.57	11.30	1.73	6	1.86	ESO162-017
NGC2369	071637.7-622037	7	2924	58	211	11.64	12.61	0.97	1	0.47	NGC2369
UGC03816	072312.4+580353	5	3369	121	137	11.27	12.70	1.43	-2	0.12	UGC03816

Table 1. Continue

Group	J2000.0	N	V_{LG}	σ_V	R_h	$\lg L/L_\odot$	$\lg M/M_\odot$	$\lg M/L$	T	Δm_{21}	Association
NGC2300	073220.5+854232	11	2100	85	409	11.45	12.86	1.41	-3	1.49	NGC2300
NGC2442	073623.8-693151	12	1135	63	150	11.24	12.24	1.00	4	1.00	NGC2442
NGC2565	081948.3+220153	5	3467	51	113	11.15	12.26	1.11	4	0.49	NGC2565
NGC2577	082243.5+223311	4	2024	108	129	10.82	12.30	1.48	-3	0.46	NGC2577
NGC2551	082450.3+732443	5	2436	51	301	10.78	12.09	1.31	0	1.03	NGC2633
NGC2594	082717.2+255244	4	2215	55	124	10.18	11.69	1.51	1	3.03	NGC2592
NGC2604A	083323.1+293220	4	2013	25	8	9.85	10.98	1.13	6	2.04	NGC2608
NGC2648	084239.8+141708	4	1933	80	94	10.78	12.17	1.39	1	2.21	NGC2648
NGC2633	084804.6+740556	5	2331	94	62	11.03	12.95	1.92	3	0.30	NGC2633
NGC2679	085132.9+305155	4	1984	61	24	10.40	11.90	1.50	-2	1.95	NGC2679
NGC2681	085332.7+511849	4	753	42	205	10.38	11.60	1.22	0	5.14	NGC2841
NGC2698	085536.5-031102	8	1673	106	94	11.11	12.78	1.67	2	0.01	NGC2698
NGC2655	085537.7+781323	8	1584	67	318	11.39	12.61	1.22	0	1.65	NGC2655
NGC2712	085930.5+445450	4	1887	41	428	10.51	12.08	1.57	3	4.51	NGC2712
NGC2719	090015.5+354340	4	3095	84	26	10.08	12.10	2.02	10	0.84	NGC2719
NGC2738	090400.5+215804	4	2979	46	108	10.73	11.58	0.85	4	0.01	NGC2738
NGC2743	090454.0+250015	4	2895	26	121	10.36	11.78	1.42	6	1.80	NGC2750
NGC2750	090547.9+252615	4	2640	170	44	10.91	13.47	2.56	5	0.14	NGC2750
NGC2775	091020.1+070217	9	1259	98	189	10.99	12.88	1.89	2	4.58	NGC2775
NGC2768	091137.5+600214	10	1416	126	315	11.28	13.09	1.81	-4	1.46	NGC2768
NGC2782	091405.1+400649	4	2512	28	30	10.86	11.89	1.03	1	4.03	NGC2782
NGC2798	091722.9+415959	6	1707	73	75	10.51	11.88	1.37	1	2.12	NGC2798
UGC04906	091739.9+525935	6	2346	49	280	10.61	12.06	1.45	1	3.21	UGC04906
NGC2855	092127.5-115434	6	1652	35	216	10.87	11.91	1.04	-0	3.77	PGC025886
NGC2841	092202.6+505836	6	640	74	233	10.78	12.61	1.83	3	5.31	NGC2841
NGC2859	092418.6+343048	8	1636	113	54	10.83	12.37	1.54	-1	3.52	NGC2859
NGC2872	092542.5+112556	11	3204	216	147	11.43	13.21	1.78	-5	0.11	NGC2911
NGC2894	092930.2+074308	6	1970	46	312	10.98	11.99	1.01	1	0.00	NGC2894
NGC2904	093017.0-302306	5	2227	74	111	10.93	12.06	1.13	-3	0.33	NGC2904
NGC2907	093136.7-164405	4	1819	109	84	10.92	12.42	1.50	1	1.64	NGC2811
NGC2903	093210.1+213003	4	417	31	69	10.42	11.62	1.20	4	5.64	NGC2903
NGC2911	093346.1+100909	21	3069	144	311	11.45	13.20	1.75	-2	0.86	NGC2911
NGC2962	094053.9+050957	8	1768	70	123	10.77	12.07	1.30	-1	1.02	NGC2962
NGC2967	094203.3+002011	6	1652	68	320	10.63	12.63	2.00	5	1.22	NGC2974
NGC2974	094233.3-034157	5	1660	66	186	11.54	13.03	1.49	-5	5.02	NGC2974
NGC2950	094235.1+585105	4	1425	44	137	10.75	12.33	1.58	-2	4.26	NGC2768
MCG+02-25-021	094253.4+092940	7	3070	47	67	10.93	11.91	0.98	3	1.04	NGC2911
NGC2964	094254.2+315050	9	1491	91	206	11.07	12.80	1.73	4	0.08	NGC2964
ESO434-028	094413.2-285055	4	2228	19	417	10.77	11.58	0.81	-3	0.92	NGC3223
NGC2986	094416.0-211641	7	2032	96	406	11.37	13.11	1.74	-5	0.66	NGC2986
NGC2997	094538.8-311128	9	785	107	126	10.86	12.63	1.77	5	3.75	NGC2997
NGC2992	094542.1-141935	4	2094	59	52	10.90	11.54	0.64	1	1.54	NGC2992
UGC05228	094603.7+014006	4	1686	38	133	10.01	11.71	1.70	5	4.57	NGC2974
NGC2990	094617.2+054232	5	2898	60	22	10.62	12.20	1.58	5	1.13	NGC2990
NGC3001	094618.7-302615	4	2139	46	488	11.08	12.35	1.27	4	0.99	NGC3223
CGCG063-066	094649.0+094410	4	2867	14	191	10.09	10.86	0.77	1	3.17	NGC2911
NGC3023	094952.6+003705	6	1670	19	28	10.24	11.21	0.97	5	0.12	NGC2974
NGC3031	095533.2+690355	30	193	138	102	10.86	12.59	1.73	2	0.81	NGC3031
NGC3078	095824.6-265537	13	2149	105	569	11.59	13.16	1.57	-5	0.46	NGC3223
UGC05376	100027.1+032228	4	1844	75	141	10.35	12.08	1.73	4	1.12	UGC05376
NGC3100	100040.8-313952	34	2420	142	738	12.08	13.57	1.49	-2	0.04	NGC3223
NGC3079	100157.8+554047	7	1205	94	122	10.88	12.26	1.38	7	3.54	NGC3079
NGC3115	100514.0-074307	5	437	58	119	10.53	12.29	1.76	-3	4.17	NGC3115
NGC3145	101009.9-122602	4	3283	62	13	11.22	11.38	0.16	4	2.84	NGC3145
ESO436-001	101247.5-275022	4	2198	71	306	10.63	12.29	1.66	4	0.29	NGC3223
NGC3166	101345.8+032530	10	1097	63	92	11.10	12.13	1.03	0	0.07	NGC3166
NGC3175	101442.1-285219	6	800	24	121	10.46	11.76	1.30	2	1.37	NGC2997
ESO567-032	101544.5-201744	6	3343	60	397	10.89	12.54	1.65	1	1.49	NGC3311
NGC3147	101653.6+732403	5	2978	80	510	11.60	12.95	1.35	4	3.42	NGC3147
NGC3190	101805.6+214955	13	1197	112	181	11.13	12.77	1.64	1	0.52	NGC4472
NGC3182	101933.0+581221	4	2203	42	321	10.57	12.00	1.43	1	1.68	NGC3182
NGC3223	102135.1-341601	53	2497	404	368	12.13	14.31	2.18	3	0.57	NGC3223
NGC3233	102157.5-221604	4	3422	57	516	11.12	12.62	1.50	0	0.82	NGC3311
NGC3227	102330.6+195154	5	1034	79	71	10.75	12.29	1.54	1	0.93	NGC4472

Table 1. Continue

Group	J2000.0	N	V_{LG}	σ_V	R_h	$\lg L/L_\odot$	$\lg M/M_\odot$	$\lg M/L$	T	Δm_{21}	Association
NGC3230	102344.0+123404	6	2728	134	111	10.94	12.49	1.55	1	3.61	NGC3230
NGC3245	102718.4+283027	6	1291	39	239	10.95	11.91	0.96	-2	0.94	NGC3245
ESO375-041	102931.0-351535	4	1476	39	58	10.07	11.16	1.09	-2	0.64	NGC3223
NGC3275	103051.8-364413	5	2852	40	674	11.29	12.44	1.15	2	1.64	NGC3223
IC2587	103059.6-343347	6	1701	91	225	10.58	12.38	1.80	-3	1.77	NGC3223
NGC3281	103152.1-345113	4	3116	135	510	11.35	13.31	1.96	2	1.72	NGC3223
NGC3282	103221.9-221808	4	3416	72	147	10.84	12.17	1.33	-2	3.50	NGC3311
NGC3266	103317.6+644458	5	1817	76	105	10.49	11.86	1.37	-2	0.51	NGC3266
NGC3300	103638.4+141016	8	2852	36	65	11.01	11.92	0.91	1	0.95	NGC3367
NGC3311	103642.8-273142	139	3303	426	520	12.51	14.29	1.78	-3	0.36	NGC3311
NGC3338	104207.5+134449	6	1123	100	86	10.55	11.54	0.99	5	1.46	NGC4472
NGC3358	104333.0-362438	7	2700	86	199	11.46	12.97	1.51	0	0.08	NGC3223
ESO501-088	104418.8-224934	8	3497	76	114	10.90	12.55	1.65	2	0.94	NGC3311
NGC3367	104635.0+134503	7	2896	57	326	11.16	12.55	1.39	5	1.52	NGC3367
NGC3379	104749.6+123454	27	747	233	179	11.47	13.23	1.76	-5	0.05	NGC4472
NGC3393	104823.5-250943	6	3450	153	382	11.35	13.28	1.93	1	1.10	NGC3311
NGC3394	105039.8+654338	10	3449	80	192	10.84	12.59	1.75	5	0.60	NGC3394
NGC3414	105116.2+275830	8	1298	117	94	10.78	12.52	1.74	-2	2.17	NGC3245
NGC3415	105142.6+434245	4	3298	53	156	11.07	12.56	1.49	-1	0.66	NGC3415
NGC3430	105211.4+325702	11	1578	103	128	10.86	12.50	1.64	5	0.15	NGC3430
NGC3449	105253.7-325539	5	2980	74	422	11.45	12.69	1.24	2	0.61	NGC3223
NGC3458	105601.5+570701	6	2000	64	74	10.62	11.98	1.36	-2	1.28	NGC3610
NGC3486	110024.0+285829	5	617	18	99	10.00	10.99	0.99	5	3.14	NGC4472
NGC3497	110718.1-192818	9	3487	144	207	11.43	12.99	1.56	-2	1.74	ESO569-024
NGC3557	110957.7-373221	13	2576	143	452	11.70	13.49	1.79	-5	1.01	NGC3557
NGC3573	111118.6-365232	5	2090	47	104	11.03	12.06	1.03	-0	0.30	NGC3557
NGC3585	111317.1-264518	9	1189	70	414	11.09	12.66	1.57	-5	3.97	NGC3585
NGC3583	111410.9+481907	5	2175	98	56	11.05	12.74	1.69	3	1.05	NGC3583
NGC3607	111654.7+180307	31	959	124	247	11.13	13.08	1.95	-3	1.10	NGC4472
NGC3610	111825.3+584710	19	1794	119	271	11.38	13.08	1.70	-4	0.66	NGC3610
NGC3613	111836.1+575960	11	2105	148	194	11.11	12.77	1.66	-5	2.47	NGC3610
NGC3626	112003.8+182125	4	1361	109	136	10.78	12.81	2.03	-1	0.67	NGC4472
NGC3627	112015.0+125930	16	728	154	192	11.43	13.05	1.62	3	0.19	NGC4472
UGC06354	112055.2+632416	4	3376	37	262	10.27	11.67	1.40	4	0.32	UGC06354
NGC3640	112106.9+031405	12	1191	174	151	10.90	12.66	1.76	-5	1.33	NGC4472
NGC3656	112338.8+535032	7	3014	109	149	10.88	12.48	1.60	1	3.53	NGC3549
NGC3665	112443.6+384546	11	2038	70	353	11.33	12.80	1.47	-2	1.45	NGC3665
NGC3672	112502.5-094743	7	1509	101	146	11.00	12.83	1.83	5	0.59	NGC3672
NGC3686	112743.9+171327	6	1044	69	114	10.55	12.22	1.67	4	0.79	NGC4472
IC0694	112831.0+583341	6	3178	73	39	11.61	13.05	1.44	4	0.18	IC0694
NGC3706	112944.4-362329	11	2684	80	280	11.38	12.85	1.47	-3	2.42	ESO320-031
IC0705	113256.3+501430	4	3104	91	99	10.20	11.99	1.79	-1	0.79	IC0705
NGC3742	113532.5-375723	8	2533	108	215	11.47	12.80	1.33	2	0.01	ESO320-031
NGC3735	113557.3+703208	4	2809	73	240	11.15	12.85	1.70	5	2.81	NGC3735
NGC3762	113723.8+614534	5	3439	71	298	11.16	12.55	1.39	1	0.73	IC0694
NGC3769	113744.1+475335	6	780	42	35	9.81	11.99	2.18	3	1.47	NGC5194
NGC3770	113758.7+593701	4	3359	139	93	10.82	12.78	1.96	1	1.14	IC0694
NGC3780	113922.4+561614	5	2484	55	415	11.04	12.68	1.64	5	0.21	NGC3780
NGC3800	114013.5+152032	4	3188	44	64	11.07	12.42	1.35	3	1.07	NGC3801
NGC3801	114016.9+174341	15	3324	82	161	11.56	12.70	1.14	-2	0.78	NGC3801
NGC3810	114058.8+112816	4	853	32	237	10.31	11.69	1.38	5	2.75	NGC4472
NGC3838	114413.8+575653	11	1368	63	202	10.60	12.19	1.59	-0	0.28	NGC5194
NGC3853	114428.3+163329	5	3218	16	436	10.91	11.60	0.69	-5	1.93	NGC3801
NGC3869	114545.6+104929	4	2868	40	347	10.89	12.09	1.20	1	2.33	NGC4472
NGC3872	114549.1+134600	8	3074	54	470	11.25	12.52	1.27	-5	2.33	NGC3801
NGC3877	114607.8+472941	21	955	65	239	11.05	12.57	1.52	5	0.03	NGC5194
NGC3894	114850.4+592456	21	3397	123	242	11.60	13.02	1.42	-4	0.74	IC0694
NGC3900	114909.5+270119	4	1745	30	227	10.74	11.31	0.57	-0	1.25	NGC4472
NGC3923	115101.8-284822	26	1553	159	357	11.62	13.33	1.71	-5	1.18	NGC3923
NGC3945	115313.7+604032	16	1399	92	358	11.28	12.93	1.65	-1	0.04	NGC3945
ESO320-031	115405.8-395150	17	2679	150	438	11.71	13.33	1.62	5	0.64	ESO320-031
NGC3966	115644.2+320118	11	3162	101	195	11.43	12.75	1.32	2	0.78	NGC3966
NGC3992	115736.0+532228	72	1097	120	452	11.68	13.33	1.65	4	0.11	NGC5194
NGC4004	115805.2+275244	4	3357	43	122	10.90	11.92	1.02	10	0.06	NGC4008

Table 1. Continue

Group	J2000.0	N	V_{LG}	σ_V	R_h	$\lg L/L_\odot$	$\lg M/M_\odot$	$\lg M/L$	T	Δm_{21}	Association
NGC4030	120023.6–010600	7	1291	50	347	10.91	12.52	1.61	4	3.57	NGC4472
NGC4039	120153.6–185311	23	1409	74	256	11.50	12.82	1.32	9	0.12	NGC4039
UGC07017	120222.5+295142	4	3100	44	123	10.56	11.70	1.14	4	1.35	NGC3966
NGC4062	120403.8+315345	4	736	33	175	10.08	11.92	1.84	5	2.55	NGC4472
NGC4105	120640.8–294537	29	1870	139	382	11.61	13.23	1.62	–4	0.60	NGC3923
NGC4111	120703.1+430355	20	851	93	212	11.14	12.69	1.55	–1	0.08	NGC5194
UGCA 272	120747.6+672302	4	2441	33	174	10.18	11.50	1.32	2	1.52	NGC4256
NGC4125	120806.0+651027	16	1515	85	282	11.33	12.67	1.34	–5	2.24	NGC3945
NGC4123	120811.1+025242	5	1150	15	80	10.36	11.15	0.79	5	1.56	NGC4472
NGC4128	120832.3+684603	4	2505	80	286	10.97	12.73	1.76	–2	2.31	NGC4256
NGC4151	121032.6+392421	16	1031	69	348	11.03	12.56	1.53	2	0.48	NGC5194
NGC4149	121032.8+581815	4	3107	51	260	10.45	12.06	1.61	3	4.98	NGC4290
NGC4150	121033.7+302406	4	211	56	56	8.68	11.61	2.93	–2	2.81	NGC4150
NGC4157	121104.4+502905	8	834	65	150	10.82	12.21	1.39	3	0.12	NGC5194
NGC4189	121347.3+132529	6	1987	30	132	10.64	11.45	0.81	6	4.83	NGC4472
ESO380–006	121534.3–353747	9	2568	147	386	11.57	13.40	1.83	3	0.50	ESO380–006
NGC4217	121550.9+470530	5	1085	55	224	10.83	12.20	1.37	3	0.55	NGC5194
NGC4216	121554.4+130858	16	55	52	23	8.60	11.24	2.64	3	2.27	NGC4472
NGC4219	121627.3–431927	4	1708	55	268	10.86	12.59	1.73	4	3.57	NGC4219
NGC4224	121633.7+072744	15	2425	118	448	11.33	12.95	1.62	1	0.18	NGC4472
NGC4250	121726.3+704809	4	2277	51	81	10.66	11.93	1.27	2	4.91	NGC4250
NGC4244	121729.7+374826	8	291	38	76	9.71	11.60	1.89	6	0.18	NGC5194
NGC4256	121843.0+655353	11	2808	157	191	11.43	12.96	1.53	3	0.99	NGC4256
NGC4254	121849.6+142459	16	2296	92	457	11.71	13.28	1.57	5	1.51	NGC4472
NGC4258	121857.5+471814	15	551	80	254	10.97	12.45	1.48	4	2.34	NGC5194
NGC4261	121923.2+054931	87	2060	276	358	11.99	13.70	1.71	–5	0.67	NGC4472
NGC4274	121950.6+293652	14	990	102	256	11.22	12.70	1.48	2	0.42	NGC4472
NGC4291	122017.8+752215	8	1866	92	337	11.12	12.76	1.64	–5	0.08	NGC4291
NGC4303	122154.9+042825	23	1387	115	434	11.35	12.97	1.62	4	1.64	NGC4472
NGC4321	122254.9+154921	17	1515	165	394	11.55	13.35	1.80	4	2.11	NGC4472
NGC4346	122327.9+465938	5	787	25	286	10.29	11.41	1.12	–2	0.95	NGC5194
NGC4342	122339.0+070314	5	596	32	125	9.87	11.44	1.57	–3	0.28	NGC4472
NGC4373	122517.8–394535	21	2992	149	554	11.95	13.40	1.45	–3	0.20	NGC4696
NGC4402	122607.6+130646	4	117	17	63	8.50	10.60	2.10	3	1.56	NGC4472
NGC4441	122720.4+644805	4	2885	49	247	10.78	12.27	1.49	–1	0.23	NGC4256
NGC4472	122946.8+080002	355	992	291	696	12.44	14.14	1.70	–5	0.34	NGC4472
NGC4490	123036.4+413837	8	583	45	98	10.36	11.84	1.48	7	1.31	NGC5194
NGC4501	123159.2+142514	31	1956	199	717	12.06	13.79	1.73	3	0.78	NGC4472
NGC4521	123247.6+635621	7	2644	68	322	10.91	12.51	1.60	0	1.86	NGC4256
NGC4527	123408.5+023914	18	1592	85	305	11.52	12.93	1.41	4	0.58	NGC4472
NGC4535	123420.3+081152	23	1747	121	624	11.75	13.36	1.61	5	0.08	NGC4472
NGC4546	123529.5–034735	4	879	49	92	10.54	12.07	1.53	–3	4.29	NGC4472
NGC4552	123539.8+123323	12	230	55	90	9.81	11.73	1.92	–5	1.79	NGC4472
NGC4565	123620.8+255916	11	1191	83	301	11.83	12.98	1.15	3	0.56	NGC4472
NGC4568	123634.3+111420	6	2163	28	135	11.59	12.25	0.66	4	0.79	NGC4472
NGC4589	123725.0+741131	4	2121	155	218	11.17	12.82	1.65	–5	2.86	NGC4291
NGC4593	123939.4–052039	7	2368	114	239	11.37	12.96	1.59	3	0.55	NGC4593
NGC4594	123959.4–113723	11	856	61	597	11.53	12.90	1.37	1	2.98	NGC4472
IC3639	124052.8–364521	4	3045	64	57	10.88	11.94	1.06	4	1.37	NGC4696
NGC4648	124144.4+742515	8	1604	52	291	10.96	12.50	1.54	–5	0.00	NGC4291
NGC4631	124208.0+323229	28	635	90	243	11.12	12.98	1.86	7	0.25	NGC4472
NGC4636	124249.9+024116	32	757	73	337	11.08	12.58	1.50	–5	1.01	NGC4472
NGC4643	124320.1+015842	9	1195	74	301	10.80	12.60	1.80	–1	4.20	NGC4472
NGC4666	124508.7–002743	16	1427	98	320	11.24	12.95	1.71	5	1.33	NGC4472
NGC4682	124715.5–100348	4	2215	48	179	10.89	12.23	1.34	6	0.10	NGC4472
NGC4690	124755.5–013922	4	2643	53	102	10.43	12.06	1.63	–3	3.79	NGC4690
NGC4697	124835.9–054803	37	1175	109	546	11.66	13.27	1.61	–5	0.13	NGC4472
NGC4696	124849.3–411840	116	2845	303	690	12.50	14.13	1.63	–4	1.08	NGC4696
NGC4750	125007.2+725228	8	1836	53	467	11.06	12.38	1.32	4	1.35	NGC4291
NGC4736	125053.1+410714	5	352	16	338	10.64	11.34	0.70	2	5.49	NGC5194
ESO507–025	125131.8–262707	26	3028	130	328	11.92	13.18	1.26	–3	0.98	ESO507–025
NGC4753	125222.1–011159	23	992	98	486	11.21	12.76	1.55	–1	1.08	NGC4472
ESO442–028	125235.2–315314	4	3315	27	175	10.60	11.80	1.20	8	3.10	ESO507–025
NGC4751	125250.8–423936	9	1838	88	254	11.10	12.85	1.75	–3	0.96	NGC4696

Table 1. Continue

Group	J2000.0	N	V_{LG}	σ_V	R_h	$\lg L/L_\odot$	$\lg M/M_\odot$	$\lg M/L$	T	Δm_{21}	Association
NGC4759	125304.5–091160	12	3471	146	454	11.81	13.55	1.74	–2	0.63	NGC4759
NGC4795	125502.9+080356	7	2548	118	53	10.80	12.34	1.54	1	0.78	NGC4472
NGC4814	125521.9+582039	5	2644	76	78	10.91	12.63	1.72	3	2.03	NGC4814
NGC4808	125549.0+041815	5	591	27	115	9.78	11.30	1.52	6	0.72	NGC4472
NGC4835	125807.8–461551	5	1933	59	83	10.92	12.31	1.39	4	4.84	NGC4696
NGC4856	125921.3–150232	5	1189	50	217	10.79	12.25	1.46	–0	3.58	NGC4472
NGC4866	125927.1+141016	5	1909	58	126	11.02	12.63	1.61	–0	3.65	NGC4472
NGC4900	130039.1+023005	8	779	36	53	9.99	11.61	1.62	5	3.35	NGC4472
NGC4902	130059.7–143049	6	2450	48	355	11.30	12.39	1.09	3	1.03	NGC5044
NGC4933B	130356.7–112953	5	3009	63	32	11.53	12.64	1.11	–0	0.02	NGC4933B
NGC4930	130405.3–412442	7	2258	75	366	10.91	12.69	1.78	4	2.71	NGC4696
NGC4936	130417.1–303135	16	2931	194	460	11.79	13.36	1.57	–5	1.70	ESO507–025
NGC4965	130709.4–281341	4	2036	30	109	10.35	11.38	1.03	7	0.11	NGC5078
NGC4995	130940.7–075000	4	1569	38	422	11.01	12.03	1.02	3	0.26	NGC4472
NGC4993	130947.7–232302	15	2702	74	375	11.42	12.44	1.02	–3	0.05	ESO507–025
NGC5005	131056.2+370333	13	986	119	171	11.24	12.85	1.61	4	0.51	NGC5194
NGC5020	131239.9+123559	6	3279	26	200	11.01	11.43	0.42	4	4.00	NGC5020
NGC5011	131251.9–430546	20	2871	131	448	11.78	13.43	1.65	–5	0.75	NGC4696
NGC5018	131301.0–193105	9	2579	133	231	11.53	12.92	1.39	–5	1.54	NGC5044
NGC5044	131524.0–162308	52	2474	245	480	11.96	13.72	1.76	–5	1.14	NGC5044
NGC5054	131658.5–163805	7	1556	101	76	11.15	12.95	1.80	4	1.01	NGC5044
IC4214	131742.7–320606	4	2109	67	495	11.03	12.80	1.77	2	2.22	NGC5078
NGC5077	131931.7–123925	9	2731	111	202	11.45	12.83	1.38	–5	1.44	NGC5044
NGC5078	131950.0–272436	26	1849	138	620	11.81	13.48	1.67	1	0.03	NGC5078
NGC5084	132016.9–214939	12	1560	141	452	11.50	13.20	1.70	–2	0.76	NGC5078
NGC5109	132052.4+573841	4	2253	44	124	10.05	11.50	1.45	4	0.24	NGC5473
NGC5090	132112.8–434216	16	3167	218	337	12.01	13.74	1.73	–5	0.58	NGC4696
NGC5121	132445.6–374056	5	1250	38	184	10.45	11.89	1.44	1	3.16	NGC5128
NGC5145	132513.9+431602	7	1310	21	226	10.40	11.44	1.04	2	0.16	NGC5194
NGC5128	132527.6–430109	15	299	94	402	11.21	12.52	1.31	–2	0.52	NGC5128
NGC5170	132948.8–175759	4	1313	86	223	10.83	12.63	1.80	5	2.57	NGC5247
NGC5194	132952.7+471143	9	574	84	182	11.29	12.93	1.64	4	0.12	NGC5194
NGC5198	133011.4+464015	15	2678	101	301	11.16	12.69	1.53	–5	1.15	NGC5198
NGC5188	133128.3–344740	6	2129	30	599	11.22	12.08	0.86	3	0.11	NGC5188
NGC5218	133210.4+624604	4	3033	55	174	11.07	12.08	1.01	3	0.66	NGC5218
UGC08603	133633.7+443557	5	2726	50	224	10.26	11.94	1.68	2	1.05	NGC5198
NGC5236	133700.9–295157	12	321	77	149	10.78	12.29	1.51	5	3.63	NGC5128
NGC5248	133732.1+085306	5	1087	48	133	10.77	12.21	1.44	4	4.91	NGC4472
NGC5297	134623.7+435219	8	2399	51	182	10.91	12.00	1.09	5	1.92	NGC5371
NGC5308	134700.4+605823	7	2172	85	191	10.93	12.59	1.66	–2	5.00	NGC5473
NGC5302	134849.7–303040	4	3444	84	210	11.37	12.58	1.21	–0	0.67	IC4296
NGC5322	134915.2+601126	21	1937	169	421	11.44	13.12	1.68	–5	1.45	NGC5473
NGC5371	135539.9+402742	55	2616	195	455	12.07	13.69	1.62	4	0.01	NGC5371
NGC5363	135607.2+051517	17	1161	143	152	11.18	12.76	1.58	0	0.87	NGC4472
NGC5383	135704.8+415048	5	2328	81	173	11.02	12.41	1.39	3	1.45	NGC5371
IC4351	135754.3–291857	5	2478	139	99	11.28	12.85	1.57	3	1.69	IC4351
NGC5403	135950.9+381057	4	2751	69	12	10.79	12.18	1.39	2	2.22	NGC5371
NGC5422	140042.0+550952	12	1935	121	249	11.07	13.01	1.94	–1	0.28	NGC5473
NGC5430	140045.7+591942	4	3158	15	418	11.07	11.14	0.07	3	1.93	NGC5430
NGC5448	140250.1+491022	5	2141	74	459	10.82	12.67	1.85	1	2.18	NGC5481
NGC5457	140312.6+542057	6	379	61	150	10.56	12.05	1.49	6	3.97	NGC5194
NGC5427	140326.0–060151	5	2496	55	89	11.17	12.59	1.42	5	0.91	NGC5427
NGC5473	140443.2+545333	18	2162	94	294	11.25	12.75	1.50	–3	0.04	NGC5473
NGC5481	140641.2+504324	9	2012	131	154	10.86	12.87	2.01	0	0.08	NGC5481
NGC5506	141314.9–031227	4	1773	29	36	10.97	11.29	0.32	1	0.92	NGC5506
NGC5529	141534.1+361336	7	2956	122	131	11.13	12.54	1.41	5	5.08	NGC5557
IC0996	141722.1+573747	4	3231	39	102	10.37	11.66	1.29	4	0.36	IC0996
NGC5557	141825.7+362937	20	3325	141	381	11.69	13.30	1.61	–5	1.56	NGC5557
NGC5566	142019.9+035601	12	1527	116	186	11.31	12.89	1.58	1	0.44	NGC5846
NGC5602	142218.8+503005	5	2354	79	103	10.57	12.23	1.66	1	1.82	NGC5676
NGC5600	142349.5+143819	4	2266	59	330	10.85	12.19	1.34	5	0.28	NGC5600
NGC5638	142940.4+031400	12	1683	84	184	10.82	12.28	1.46	–5	3.03	NGC5846
NGC5661	143157.4+061502	4	2303	48	79	9.99	11.66	1.67	6	1.62	NGC5661
NGC5678	143205.6+575517	7	2081	78	196	11.20	12.67	1.47	3	0.18	NGC5473

Table 1. Continue

Group	J2000.0	N	V_{LG}	σ_V	R_h	$\lg L/L_\odot$	$\lg M/M_\odot$	$\lg M/L$	T	Δm_{21}	Association
NGC5643	143240.8–441029	4	986	59	167	10.92	12.48	1.56	5	0.70	NGC5643
NGC5676	143246.8+492728	17	2389	105	348	11.57	12.99	1.42	5	0.48	NGC5676
NGC5707	143730.8+513343	7	2348	87	220	10.73	12.12	1.39	2	2.26	NGC5676
UGC09476	144132.0+443046	4	3401	23	100	10.77	11.76	0.99	5	0.56	UGC09476
NGC5729	144206.9–090034	4	1750	49	106	10.43	11.76	1.33	3	1.71	NGC5729
NGC5726	144256.0–182642	4	3333	54	134	10.81	12.02	1.21	–3	3.29	NGC5726
IC1048	144258.0+045322	4	1671	59	132	10.27	11.98	1.71	3	2.42	NGC5846
ESO512–018	144333.9–242739	6	3321	168	103	11.33	13.09	1.76	–2	1.09	ESO512–018
NGC5746	144456.0+015717	39	1679	107	269	11.66	13.20	1.54	3	1.36	NGC5846
ESO580–027	144728.5–221642	4	3169	20	174	10.96	11.53	0.57	1	1.49	ESO512–018
NGC5757	144746.4–190443	6	2532	46	268	11.10	12.05	0.95	3	0.75	NGC5728
NGC5775	145357.6+033240	8	1558	105	129	11.07	12.85	1.78	5	1.43	NGC5846
NGC5792	145822.7–010528	6	1822	50	290	11.06	12.03	0.97	3	4.19	NGC5846
NGC5820	145839.8+535310	5	3423	83	218	11.11	12.47	1.36	–2	1.50	NGC5908
NGC5791	145846.2–191601	11	3257	129	309	11.51	13.11	1.60	–4	1.13	NGC5791
NGC5796	145924.1–163726	7	2901	223	375	11.54	13.37	1.83	–5	1.22	NGC5796
NGC5812	150055.7–072726	4	1829	140	132	11.02	12.37	1.35	–5	1.97	NGC5812
MCG–02–38–030	150300.2–131658	5	2697	130	187	10.98	13.27	2.29	1	0.45	NGC5796
NGC5838	150526.3+020558	9	1266	54	148	11.01	12.16	1.15	–3	0.87	NGC5846
NGC5846	150629.3+013620	74	1809	228	395	11.80	13.64	1.84	–5	0.46	NGC5846
NGC5861	150916.1–111918	5	1825	107	295	10.89	12.22	1.33	5	0.45	NGC5861
NGC5907	151553.7+561944	10	950	66	265	11.17	12.54	1.37	5	0.11	NGC5907
NGC5898	151813.6–240553	14	2233	187	131	11.49	13.09	1.60	–4	0.03	NGC5898
NGC5930	152607.9+414034	8	2784	85	81	11.16	12.65	1.49	2	0.98	NGC5899
NGC5961	153516.2+305152	4	1887	58	70	9.96	12.04	2.08	3	2.41	NGC5961
NGC5962	153631.7+163628	5	2020	31	51	11.07	11.98	0.91	5	0.63	NGC5962
IC1128	153752.9–014407	5	3430	76	172	10.74	12.38	1.64	–2	1.18	IC1128
NGC5982	153839.8+592121	16	3123	159	512	11.82	13.31	1.49	–5	0.00	NGC5982
NGC6000	154949.6–292313	4	2094	30	182	10.99	11.01	0.02	4	3.93	NGC6000
NGC6181	163221.0+194936	4	2571	61	204	11.09	12.29	1.20	5	1.61	NGC6181
NGC6307	170740.5+604503	4	3312	55	81	10.96	12.06	1.10	2	1.37	NGC6307
NGC6340	171024.9+721816	6	1492	59	101	10.72	12.06	1.34	0	1.50	NGC6340
IC4633	171347.0–773210	6	2736	96	161	11.43	12.91	1.48	6	0.72	IC4633
NGC6484	175147.0+242900	4	3363	38	174	10.96	11.74	0.78	2	1.47	NGC6427
NGC6501	175603.7+182223	7	3312	137	185	11.50	13.20	1.70	–1	0.05	NGC6501
IC4704	182753.6–713635	6	3429	173	287	11.62	13.08	1.46	–3	0.59	IC4704
IC4797	185629.7–541821	8	2641	150	179	11.63	13.15	1.52	–4	0.26	IC4797
NGC6744	190946.1–635127	9	751	78	229	11.12	12.59	1.47	4	1.11	NGC6744
NGC6753	191123.6–570258	5	2954	106	587	11.57	13.20	1.63	3	3.12	IC4797
NGC6758	191352.3–561836	7	3355	111	434	11.60	13.12	1.52	–4	1.00	IC4797
NGC6868	200954.1–482246	19	2780	182	309	11.96	13.38	1.42	–5	0.39	NGC6868
NGC6903	202344.9–191932	5	3449	50	389	11.38	12.51	1.13	–3	3.53	NGC6903
NGC6902	202428.1–433913	7	2958	155	246	11.41	13.07	1.66	2	0.12	NGC6868
NGC6907	202506.7–244834	4	3216	32	726	11.43	12.03	0.60	4	2.10	NGC6907
IC5011	202833.8–360138	4	2391	59	34	10.95	11.56	0.61	–2	2.66	IC5011
NGC6925	203420.6–315851	6	2862	105	296	11.50	13.17	1.67	4	0.82	NGC6925
IC5063	205202.3–570408	4	3303	64	172	11.26	12.25	0.99	–1	1.38	IC5063
IC5096	211821.5–634538	5	2984	125	453	11.56	13.23	1.67	4	0.37	IC5096
NGC7049	211900.2–483343	5	2136	138	185	11.55	13.16	1.61	–2	0.97	NGC7049
ESO287–013	212313.9–454623	4	2710	64	84	10.85	12.26	1.41	4	1.80	NGC7079
NGC7126	214918.1–603633	5	2946	58	87	10.86	11.95	1.09	5	0.46	NGC7126
NGC7144	215242.4–481513	5	1830	34	384	11.26	11.91	0.65	–5	0.55	NGC7213
NGC7166	220032.9–432323	6	2385	140	95	11.18	13.03	1.85	–3	1.01	NGC7166
NGC7176	220208.5–315923	22	2633	139	190	11.75	13.11	1.36	–5	0.31	NGC7176
NGC7185	220256.7–202817	4	1899	22	195	10.40	10.66	0.26	–3	1.27	NGC7185
NGC7196	220554.8–500710	4	2820	58	61	11.30	12.85	1.55	–5	1.69	NGC7196
NGC7192	220650.2–641858	5	2835	59	441	11.38	12.73	1.35	–4	1.07	IC5250A
NGC7213	220916.3–471000	11	1806	126	180	11.55	13.16	1.61	1	1.14	NGC7213
IC5179	221609.1–365037	5	3424	87	404	11.25	12.64	1.39	4	2.91	IC5179
IC1438	221629.1–212550	5	2716	24	356	10.82	11.66	0.84	1	2.92	IC1438
NGC7302	223223.8–140714	4	2822	94	26	10.90	12.52	1.62	–3	3.98	NGC7302
NGC7331	223704.1+342456	4	1113	44	276	11.29	12.34	1.05	4	4.50	NGC7331
IC5250A	224717.5–650335	11	3076	90	192	11.83	13.23	1.40	–3	0.12	IC5250A
NGC7410	225501.0–393941	5	1871	170	273	11.28	13.41	2.13	3	2.79	NGC7582

[t]

Table 1. Continue

Group	J2000.0	N	V_{LG}	σ_V	R_h	$\lg L/L_\odot$	$\lg M/M_\odot$	$\lg M/L$	T	Δm_{21}	Association
IC1459	225710.6–362744	16	1775	221	336	11.66	13.54	1.88	−5	1.57	NGC7582
IC5267	225713.6–432346	5	1644	93	185	11.21	12.48	1.27	−1	1.14	NGC7582
UGC12281	225912.8+133624	4	2871	39	85	9.73	11.18	1.45	7	2.33	UGC12281
NGC7454	230107.3+162258	7	2248	83	86	10.85	12.46	1.61	−5	0.06	NGC7454
NGC7484	230704.9–361631	4	2707	103	40	10.95	12.37	1.42	−5	3.38	NGC7484
NGC7507	231207.6–283223	4	1605	80	57	11.18	12.00	0.82	−5	1.67	NGC7507
NGC7582	231823.5–422214	13	1578	67	299	11.64	12.61	0.97	2	0.22	NGC7582
IC5328	233316.5–450057	6	3084	67	566	11.29	12.82	1.53	−4	3.52	IC5328
NGC7716	233631.5+001750	5	2797	40	291	10.81	11.79	0.98	3	2.49	NGC7716
NGC7727	233953.9–121735	5	2043	51	314	11.37	12.19	0.82	1	0.59	NGC7727
NGC7743	234421.1+095603	4	1856	81	94	11.03	12.29	1.26	−1	0.22	NGC7743

Figure 1. Sky distribution of the groups in equatorial coordinates. The groups are plotted as circles with a diameter proportional to the group K -band luminosity. The circle colour indicates a morphological type of the main galaxy in the group. The upper, middle and bottom panels corresponds, respectively, to three different volumes separated by the mean radial velocity of the groups. Small dots present the distribution of individual galaxies with radial velocities in the above intervals. The zone of strong Galactic extinction is shown in grey.

5 BASIC PROPERTIES OF THE GROUPS

The distribution of groups of galaxies over the sky in equatorial coordinates is given in three panels of Fig. 1. The upper, middle and bottom panels correspond to near, intermediate and far volumes, delimited by the mean radial velocities of the groups: $V_{LG} < 1200 \text{ km s}^{-1}$, $1200 < V_{LG} < 2400 \text{ km s}^{-1}$ and $2400 < V_{LG} < 3500 \text{ km s}^{-1}$. Each group is indicated by a circle, the diameter of which is proportional to the total K -luminosity (i.e. the stellar mass) of the group members. The circle colour indicates the morphological type of the main member of the group in the colour spectrum: from the early E, S0 types with an old population (red) to the late Irr, BCD types with a young population (light blue). For comparison, small black dots show the distribution of individual galaxies with radial velocities in the above intervals. The grey ragged ring-shaped region traces the zone of strong absorption in the Milky Way according to Schlegel et al. (1998).

As expected, a complex of groups in the Virgo region, where the core of the Local Supercluster of galaxies is located, stands out in the near volume ($V_{LG} < 1200 \text{ km s}^{-1}$). The richest group ($n = 355$ members) is associated with a giant elliptical galaxy M 49 = NGC 4472. The neighbouring groups with the total number of members amounting to 1558 are located mostly along the equator of the Local Supercluster. The other most massive groups in this volume are the groups around M 105 = NGC 3379 (Leo I) and NGC 1553 (Dorado). Among the nearest groups our criteria identifies practically all the known groups around the main galaxies: M 81, NGC 253, Cen A, M 83, NGC 628, M 51, M 101, NGC 891/1023, M 104 (Sombrero) etc.

In the intermediate volume ($1200 < V_{LG} < 2400$) the traces of group concentration within the Virgo region are also visible, but in general the effect of the Local Supercluster is barely noticeable. The most massive group in this volume is the Fornax cluster (NGC 1399) with a population of $n = 111$. The aggregate of groups in the Fornax and in the Eridanus (NGC 1332/1395/1407) gathers 379 galaxies in total. In addition to these, in other regions of the sky

there are massive groups around NGC 5846 ($n = 74$) and NGC 5746 ($n = 39$).

In the distant part of the studied volume (the bottom panel of Fig. 1) the groups show a tendency to be located along some filaments. The most massive groups: Centaurus (NGC 4696), Antlia (NGC 3268) and Hydra (NGC 3311) have masses comparable with that of the Virgo and Fornax clusters. It is easy to notice that the colour of circles in all the panels is correlated with their sizes, demonstrating the well-known observational fact that the E and S0 galaxies usually occur among the brightest members of rich groups and clusters.

Increasing the clustering parameter κ in (5), the galaxies can be combined into more extended aggregates (clouds), which no longer meet the condition of virial equilibrium. However, the members of such associations still probably lie within their common ‘zero-velocity surface’, i.e. they will approach each other and be subjected to the subsequent virialization. Three panels in Fig. 2 show the distribution of galaxies in the sky with radial velocities in the same intervals as in Fig. 1. The shaded polygons there represent the zones of such aggregates with their real angular sizes in the sky. In the nearby volume (the top panel) the most extended aggregate is the Virgo cluster, and its angular diameter is approximately equal to the diameter of the ‘zero-velocity surface’ of the cluster, which is $2R_0 = 46^\circ$ according to Karachentsev & Nasonova (2010). In the middle panel in the volume of $1200 < V_{LG} < 2400 \text{ km s}^{-1}$, the most extended aggregate is the Fornax+Eridanus association of groups. Its angular size is also close to the diameter $2R_0$, which is equal to $\simeq 22^\circ$ as estimated by Nasonova et al. (2011). These correspondences suggest that the dimensions of other associations (overdensities) from Fig. 2 may be also in accordance with sizes of their ‘infall zones’. It will be appropriate to note here that there is a significant fraction of galaxies that are located outside the volumes of both groups and clouds. Their distribution does not appear to be random, but shows some correlation with the distribution of group centres. The most isolated of these ‘field galaxies’ (Karachentsev et al. 2009)

Figure 2. Sky distribution of the galaxy associations identified by the clustering algorithm with $\kappa = 40$. The shaded polygons outline real angular sizes of the systems. Three panels correspond to the same volumes as in Fig. 1.

are of considerable interest with regard to the effect of their isolation on the population and structure of these objects, and the star formation rate in them.

Among 10914 galaxies in the studied volume, the individual distance estimates are so far known for less than 2000 galaxies. Most of them are spiral galaxies, where the distances were determined by the Tully & Fisher (1977) method with the accuracy of ~ 20 per cent from the relation between the luminosity and rotation amplitude of the galaxies. However, to ensure a uniform approach we used only the Hubble distances of galaxies $D = V_{LG}/H_0$, that, of course, distorts the true picture of distribution of galaxy groups in the Local universe. The distribution of 395 identified groups by their mean radial velocities is presented in Fig. 3. The groups in which the main member is a galaxy with a well-developed bulge ($T \leq 2$) are marked in the figure in grey. As one can see, the distribution of $N(V_{LG})$ is markedly different from homogeneous, showing an excess of the group number from the Virgo and Fornax complexes with their velocities around 1500 km s^{-1} . In the Local Volume ($V_{LG} < 750 \text{ km s}^{-1}$) there exists a lack of groups with the main galaxies of early type. It reflects the well known effect of the morphological segregation with environment because our Galaxy lies on the edge of Local Supercluster far away from the dense concentration of the galaxies.

Fig. 4 shows the distribution of groups by their radial velocity dispersion. The value σ_V in groups ranges from 10 to 450 km s^{-1} with the median of 74 km s^{-1} . In the groups where the main galaxy belongs to the E, S0, Sa types, the median dispersion (82 km s^{-1}) is slightly higher than in the groups with the late-type main galaxy (61 km s^{-1}). Since in the modern optical redshift surveys the typical velocity measurement errors amount to $\sim 40 \text{ km s}^{-1}$, their effect on the virial motion amplitude is significant. The groups, presented in the tail of the distribution are in general those, dominated by the early-type galaxies; they are marked in the figure in grey.

According to data from Fig. 5, the mean projected radius of the groups is distributed over a wide range from 33 kpc to 903 kpc with a median of 268 kpc. The groups with a dominant early-type galaxy (shown in grey) have the linear size on the average slightly larger (276 kpc) than the others (256 kpc). It is obvious that the observed diversity of linear sizes of groups has a physical origin, rather than being caused simply by the projection factors.

A two-dimensional distribution of 395 groups by linear dimension and velocity dispersion is presented in the left panel of Fig. 6. Despite a large scatter, a weak positive correlation between σ_V and $\langle R \rangle$ is visible. A straight line in the lower right corner indicates the region where the ‘crossing time’ of the group exceeds the Hubble time of the Universe $H_0^{-1} \text{ Gyr}$. Only 3 per cent of all groups outreaches this limit mainly due to the projection factors. The right panel in Fig. 6 depicts a similar distribution, but with the radial velocity dispersion normalized over the total K -luminosity of the group. The straight line corresponds to the case where the velocity dispersion is proportional to the linear size of

the group, $\sigma_V \propto \langle R \rangle$, and the integral luminosity of the group is proportional to its volume, $L_K \propto \langle R \rangle^3$.

Fig. 7 shows how the total K -luminosity (left) and projected mass (right) change with an increasing number of group members. Solid and open circles denote, respectively, the systems with a bulge-dominated and disc-shaped main members. The straight lines in the panels correspond to the linear regressions: $\log L_K \propto 1.01 \lg n$ and $\log M_p \propto 1.38 \lg n$, different slopes of which indicate that the mass of the group grows with the population faster than its luminosity. It might imply that either the baryon fraction is lower in more massive groups or, more plausibly, that the cumulative star-formation efficiency is lower.

As we have noted, modern optical surveys provide an insufficient accuracy of radial velocity measurements even for relatively nearby galaxies. This is reflected in a noticeable way on the estimates of group masses. A histogram of the distribution of the number of groups over the logarithm of the projected mass is demonstrated in the left panel of Fig. 8. The distribution has a fairly symmetrical shape with the median $3.3 \cdot 10^{12} M_\odot$. Here the median mass of the groups which are dominated by early-type galaxies (the grey part of the histogram) amounts to $4.0 \cdot 10^{12} M_\odot$. A transition to the unbiased mass estimates via a quadratic subtraction from σ_V^2 of the velocity measurement errors reduces the median to $2.3 \cdot 10^{12} M_\odot$. A similar effect manifests itself in the distribution of groups by the value of the projected mass-to-luminosity ratio (right panel in Fig. 8), where the medians of the biased and unbiased estimates are 31 and $22 M_\odot/L_\odot$, respectively. Thus, neglecting the real accuracy of galaxy velocity measurements, one overestimates the mass of groups on the average by 30 per cent. Someone might suspect the discrepancy between adopted value $\kappa = 6$, based on training the group-finding algorithm in the Local Volume, and the derived value of $M/L_K = 22$ from the groups found with this algorithm. There is no contradiction here. The criterion (3–4) does not use any assumptions about projection effects. These inequalities are true for observable values because projection only decreases real separation and velocity difference between galaxies. For virialized systems the projection factor is $3\pi/2$ for criterion 3. Thus the expected value of M/L_K is about 28 that is in good agreement with derived value of mass-to-light ratio.

The relations between the projected mass of the group and its luminosity L_K , as well as its linear size $\langle R \rangle$ are represented in the panels of Fig. 9. The lines of robust regression weighted by dispersion of scatter in the left and right panels are $\lg M_p \propto 1.15 \pm 0.03 \lg L_K$ and $\lg M_p \propto 2.0 \pm 0.1 \lg \langle R \rangle$, respectively. Here the correlation of the mass M_p with the linear size of a group is significantly less pronounced than with the luminosity.

Fig. 10 demonstrates the distribution of 395 groups by the total luminosity L_K and by the projected mass-to-luminosity ratio. The groups, where the dominant galaxy belongs to the early types $T \leq 2$ are shown with solid circles, and the rest of groups — with open circles. The size of the circles is proportional to the group population. The horizontal dotted line captures the ratio $M/L_K = 97 M_\odot/L_\odot$,

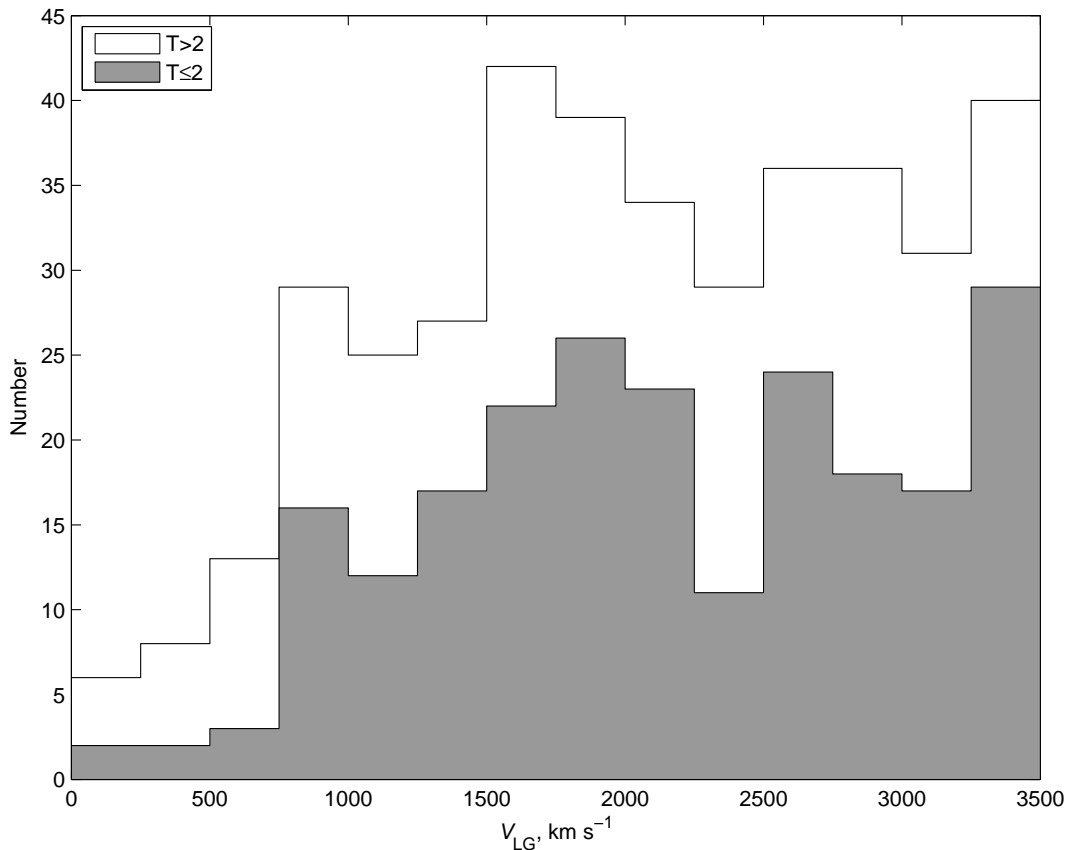


Figure 3. Distribution of 395 identified groups by their mean radial velocities. The groups with a bulge-dominated principal galaxy ($T \leq 2$) are shown in grey.

which corresponds to K -luminosity density $j_K = 4.28 \cdot 10^8 L_\odot \text{ Mpc}^{-3}$ (Jones et al. 2006) assuming Hubble constant $H_0 = 73 \text{ km s}^{-1} \text{ Mpc}^{-1}$ and the cosmic parameter of matter density $\Omega_m = 0.28$ in the standard λ CDM model.

We can see that the region of low values $M_p/L_K < 5 M_\odot/L_\odot$ is occupied by the groups with the population $n = 4-6$. An example of this is a group around the spiral galaxy NGC 660 with $R_h = 235 \text{ kpc}$ and velocity dispersion of only 29 km s^{-1} . In the region of high values $M_p/L_K > 97 M_\odot/L_\odot$ there are 10 groups, most of which with $n = 4-6$ members are in this region due to a random projection factors game. In fact, only one group in the zone $M_p/L_K > 97$: NGC 3223 (Antlia) is a massive group (cluster) with a big number of measured radial velocities, $n=53$. In addition, the region of values $M_p/L_K > 97$ contains three groups with low luminosities: NGC 4216 ($n=16$), NGC 4402 ($n=4$) and NGC 4150 ($n=4$). The first two groups are located in the Virgo cluster core and have mean radial velocities of $+55 \text{ km s}^{-1}$ and $+117 \text{ km s}^{-1}$, respectively. Consistent with these velocities, the distances and luminosity of these groups are anomalously low, what led to their fictitiously high M_p/L_K ratios. The disadvantage of our algorithm, where the distance of a group is determined by the mean radial velocity of its galaxies, is most pronounced in the regions with large peculiar motions. Some groups we identified in the Virgo cluster core are, most probably, false groups, rather than physical subsystems in the Virgo cluster. The highest value $M_p/L_K = 843 M_\odot/L_\odot$ falls within

the group of 5 galaxies around NGC 4150 in the Coma I region. The mean radial velocity of the group, $+211 \text{ km s}^{-1}$, corresponds to the distance of 2.9 Mpc, whereas the individual distances of NGC 4150 and the other members are 4–5 times more distant. It is likely that these galaxies with low radial velocities have a large component of peculiar velocity, moving towards the Virgo cluster.

The line $\lg M_p/L_K \propto 0.15 \lg L_K$ on Fig. 10 corresponds to correlation between mass and luminosity from Fig. 9. It shows that the mass-luminosity ratio of a group on the average increases from poor to rich groups. Interestingly, its intersection with the $\Omega_m = 0.28$ line can occur for group with luminosity $L_K \simeq 3 \cdot 10^{14} L_\odot$, which is comparable with total luminosity of the Local Supercluster.

An important parameter of galaxy system is the crossing time. Taking into account the effects of projection the crossing time is

$$t_{cr} = \frac{4}{\pi\sqrt{3}} \frac{\langle R_\perp \rangle}{\sigma_V}. \quad (7)$$

where the mean projected pairwise separation, R_\perp , is characteristic size and the velocity dispersion, σ_V , is characteristic inner motion in the group. The distribution of 395 groups by t_{cr} , presented in Fig. 11, has a fairly symmetrical shape with the median at 3.8 Gyr. The groups with a dominant E, S0, Sa galaxy (hatched) are characterized by a slightly shorter crossing time (3.4 Gyr) than the others (4.1 Gyr). Only 3 per cent of groups fall into the region $t_{cr} > 13.7 \text{ Gyr}$.

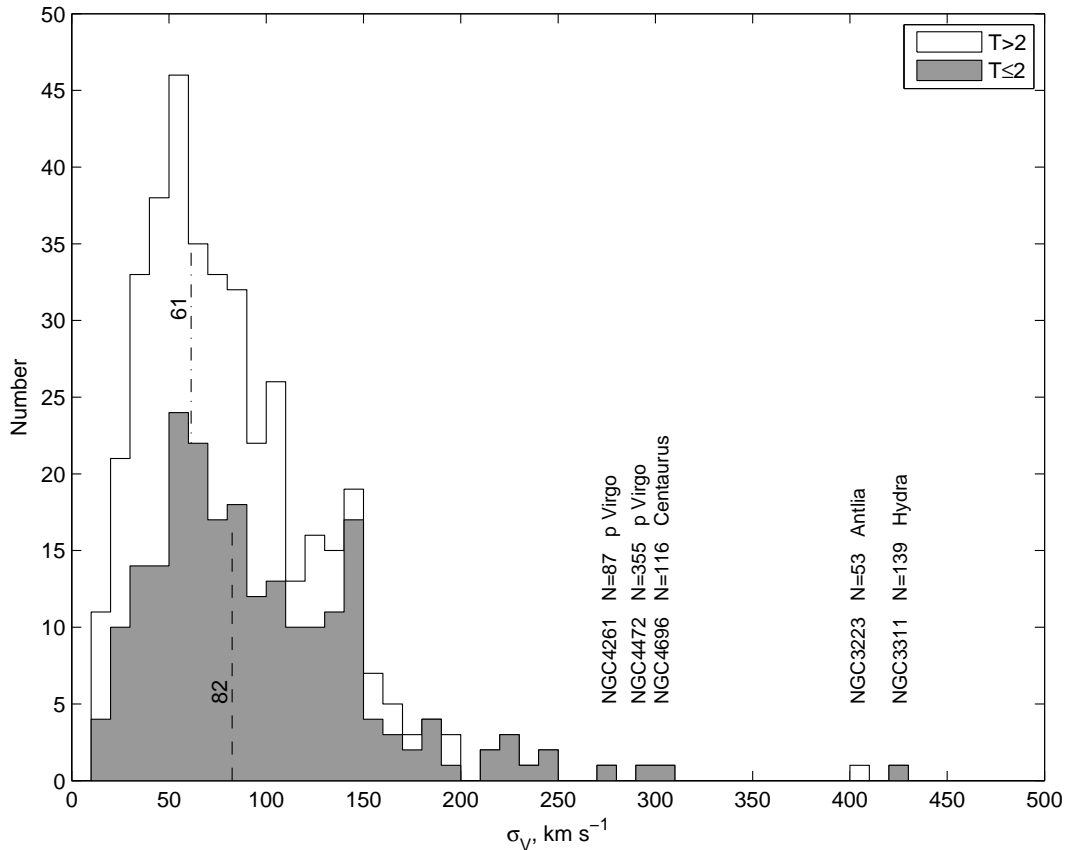


Figure 4. Distribution of the groups by their radial velocity dispersion. The groups with a bulge-dominated main galaxy is shaded.

The correction for velocity error increases this value up to 19 per cent. Consequently, the essential fraction of the groups selected by our criterion can be considered as dynamically evolved systems.

6 DISCUSSION

As the data in Fig. 12 show, the radial velocity dispersion and the linear diameter of group trend to increase slightly with distance. However, the mean projected mass-to-luminosity ratio (corrected or uncorrected for velocity measurement errors) practically does not depend on the distance. In other words, the physical requirements we used for galaxy clustering (the negative value of the total energy of a virtual pair, and its component separation to be within the radius of the zero-velocity surface) appear to be weakly sensitive to a loss of dwarf galaxies, which increases with a distance. Therefore, our criterion does not need special tuning of dimensionless parameter κ as a function of the group distance.

It should be remind that the population of groups n , presented in our catalogue, corresponds to the number of group members with already measured radial velocities. Besides these galaxies, the group volume may contain a lot of dwarf galaxies without radial velocity estimates. Such dwarf systems (dSph and dIrr), usually having a low surface brightness, were found in large quantities in nearby ($D \leq 15$ Mpc) groups by Karachentseva & Karachentsev

(1998); Karachentsev & Karachentseva (2004); Karachentsev et al. (2007) at the visual examination of the POSS-II prints. Recently, Eigenthaler & Zeilinger (2010) used the SDSS survey data to search for dwarf members of the NGC 5846 group. Mahdavi et al. (2005); Tully & Trentham (2008); Trentham & Tully (2009) looked for the dwarf population in the groups NGC 5846, NGC 5353/4 and NGC 1023, using high-resolution images taken with the MegaCam CCD camera on the CFHT telescope. A large number of dwarf members in the Virgo and Fornax clusters were found by Binggeli et al. (1985); Ferguson (1989); Ferguson & Sandage (1990); Mieske et al. (2007). The physical membership of these objects needs to be confirmed via the distance and/or radial velocity measurements. A consolidated list of the most probable dwarf galaxies in the nearby groups from our catalogue as potential targets for measuring new radial velocities is under preparation by Karachentseva et al. (2011).

A comparison of galaxy membership in our groups with its affiliation in groups in other catalogues is quite difficult to perform due to essential differences in the volumes of space covered by different catalogues, as well as the sets of original data on radial velocities of galaxies used, which are rapidly growing with time. Nevertheless, well-known groups, such as NGC 5371, NGC 5846, show a fairly detailed agreement in their member composition.

Using the data of ‘A Catalog of Neighboring Galaxies’ (CNG) (Karachentsev et al. 2004), which presents individual distances to many galaxies with $D < 10$ Mpc, and indicates

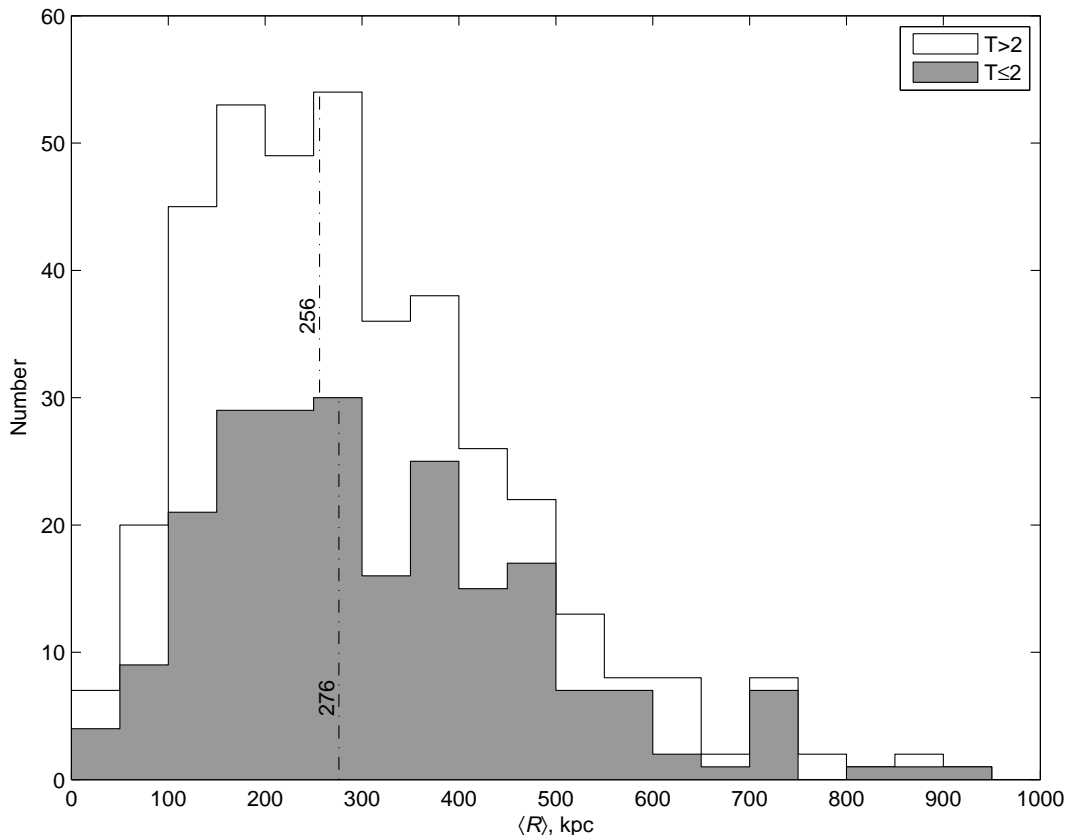


Figure 5. Distribution of the identified groups by their mean projected radius. The groups with a bulge-dominated main member are shown in grey.

in the comments their membership in the nearby groups, we compared the populations of these groups in the old (n_{CNG}) and new (n_{MK}) catalogues. As we can see from Fig. 13, for the majority of 23 nearby groups there is a good agreement between the numbers of group members. An exception is a group of galaxies NGC 4278 (Coma I), which is located in a complex region near Virgo, where several groups overlap at the equator of the Local Supercluster and a significant role is played by the Virgocentric infall effect. It should be emphasized, however, that a comparison we made generally refers to a rather ‘cold’ region of the Local Volume. An application of our algorithm to the cluster zones (Virgo, Fornax) with large non-Hubble velocities can generate fictitious, phantom groups.

Some authors (Jones et al. 2003; Díaz-Giménez et al. 2008; von Benda-Beckmann et al. 2008) propose to distinguish a special category of ‘fossil’ groups, where the main galaxy significantly surpasses all the other members on the luminosity scale. The dynamical evolution of such groups could have evolved on a different scenario than that of other groups. An example of a ‘fossil’ group in the Local Volume can be a group of companions around M 104 (Sombrero), where the K-magnitude difference between the second and the first brightest galaxies is $K_2 - K_1 = 2.98^m$, or M 101 with the difference of $K_2 - K_1 = 3.97^m$. The NGC 2903 group has the biggest difference in the Local Volume, $K_2 - K_1 = 5.64^m$. The groups around M 51 ($K_2 - K_1 = 0.12^m$), NGC 4244 (0.18^m), NGC 55 (0.13^m), Cen A (0.52^m) and M 81 (0.81^m)

are located at the opposite end of the $K_2 - K_1$ scale in the Local Volume. If we attribute as fossil groups those with $K_2 - K_1 > 2.50^m$, then our catalogue contains 81 such groups or 21 per cent of their total number. Two upper panels in Fig. 14 show the distribution of 395 groups by linear size $\langle R \rangle$ and integral luminosity L_K . Here the fossil groups are given in grey. The third panel exhibits a relation between the projected mass-to-luminosity ratio and $K_2 - K_1$. The fossil groups with $K_2 - K_1 > 2.50^m$ tend to have a bit lower mean size, luminosity and M_p/L_K ratio than the others.

As noted above, our algorithm of galaxy clustering is not entirely reliable in the ‘hot’ areas with large non-Hubble motions. In the Virgo as in the core of the Local Supercluster our criterion identifies 46 groups and pseudogroups. At a lower density contrast with the parameter $\kappa = 40$ they all merge into the association M 49, which is easily tracked in column (12) Table 1. In general this association (i.e., the Virgo cluster) contains 1558 galaxies with a total luminosity of $L_K(\text{Virgo}) = 1.4 \cdot 10^{13} L_\odot$ and the projected mass sum of $\Sigma M_p(\text{Virgo}) = 6.0 \cdot 10^{14} M_\odot$. This mass is close to the total virial mass of Virgo as a single dynamic aggregate $M_{VIR} = (7 \pm 1) \cdot 10^{14} M_\odot$ according to Hoffman et al. (1980); Tully & Shaya (1984); Tonry et al. (2000). Note as well that for the conglomerate of the groups identified by us in the Virgo cluster, the ratio $\Sigma M_p / \Sigma L_K = 43 M_\odot / L_\odot$ practically coincides with the virial estimate $M_{VIR} / L_K = (48 \pm 6)$

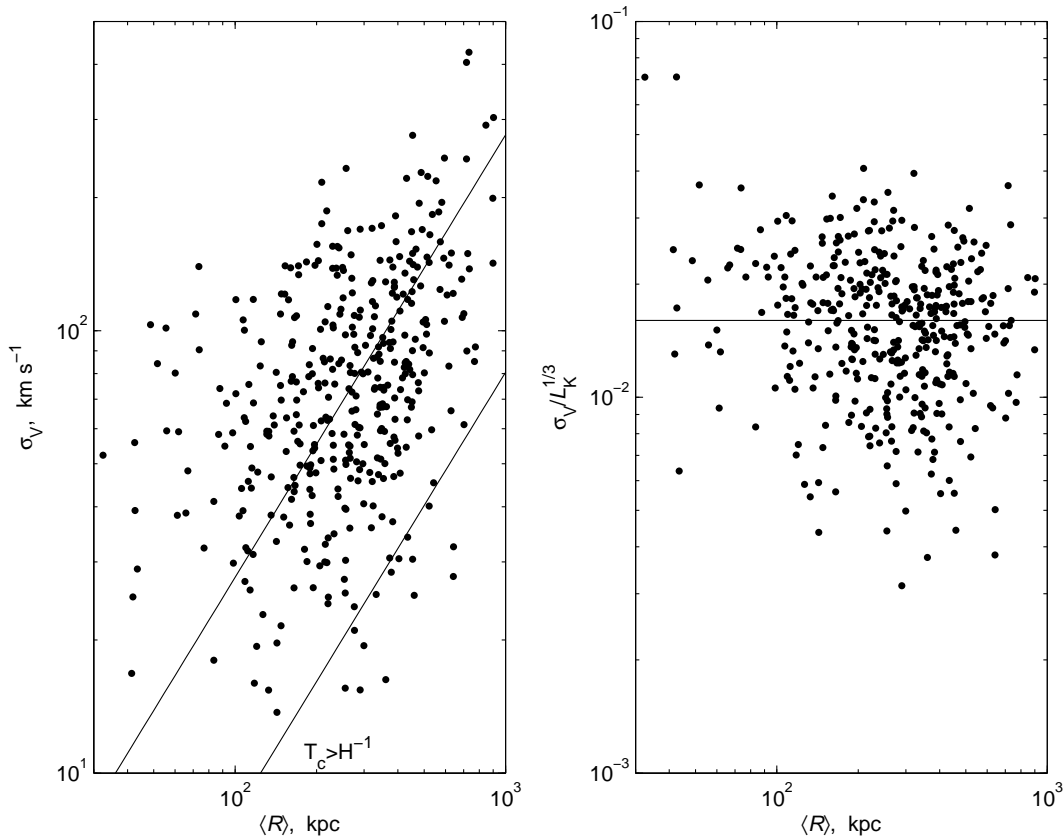


Figure 6. Left: radial velocity dispersion versus mean projected radius for the identified groups. Right: the radial velocity dispersion normalized over the total K -luminosity of the group.

M_{\odot}/L_{\odot} , obtained by McLaughlin (1999) within the radius 1.8 Mpc.

In the region of another nearby cluster, Fornax, our algorithm identifies 27 multiple systems with the total number of members equal to 379, which at the low density contrast ($\kappa = 40$) join into the association NGC 1399=Fornax (see the last column of Table 1). The total luminosity of the Fornax+Eridanus association is $\Sigma L_K(\text{For} + \text{Eri}) = 5.0 \cdot 10^{12} L_{\odot}$, and the sum of projected masses of 27 systems is $\Sigma M_p(\text{For} + \text{Eri}) = 2.1 \cdot 10^{14} M_{\odot}$. The ratio of these quantities, $\Sigma M_p / \Sigma L_K = 43 M_{\odot}/L_{\odot}$ is somewhat higher than the ratio $32 M_{\odot}/L_{\odot}$, obtained by Desai et al. (2004) for the Fornax cluster itself at $L_K(\text{Fornax}) = 1.8 \cdot 10^{12} L_{\odot}$ and $M_p(\text{Fornax}) = 5.9 \cdot 10^{13} M_{\odot}$.

We assume that among the 27 multiple systems identified by us in the Fornax+Eridanus region, the majority are real substructures of the complex that have not yet reached dynamic equilibrium. Interestingly, the group NGC 1386 with the mean radial velocity $+755 \text{ km s}^{-1}$ has the greatest value in the complex, $M_p/L_K = 106 M_{\odot}/L_{\odot}$. The corresponding Hubble distance to the group is 10.3 Mpc. However, Tonry et al. (2001) determined the individual distances to three galaxies in this group: NGC 1386, NGC 1395 and E 358-59, and the mean distance deduced from them is $(19.3 \pm 1.6) \text{ Mpc}$. Obviously this group is falling from the far side onto the Fornax cluster. With a more precise distance, the projected mass-to-luminosity ratio of NGC 1386 group drops to $57 M_{\odot}/L_{\odot}$.

A comparison between two rich complexes in the Virgo and Fornax+Eridanus yielded the ratio of the galaxy number in them as 4.1, the ratio of the total K -luminosities as 2.7, and the ratio of projected masses as 2.8. As a curiosity, note that Crook et al. (2007) estimated the ratio of the projected masses as $M_p(\text{Virgo})/M_p(\text{For} + \text{Eri}) = 0.23$, what is contrary to numerous observational data.

As the most massive structure within the distance of $D = 40 \text{ Mpc}$, the Virgo cluster amounts to 18 per cent of galaxies in this volume, 15 per cent of the total K -luminosity and 15 per cent of the projected mass. Such a proportion of baryons as well as dark matter contained in rich clusters is quite consistent with the generally accepted ideas.

In Table 1 the group of 9 galaxies around M 51 stands out among the remaining 394 groups due to its weak isolation. The clustering of galaxies into associations at a low density contrast results in a sharp increase in the number of galaxies, joining this group. Being a group of middle compactness with $R_h = 182 \text{ kpc}$, and uniting with other groups: NGC 4244, NGC 4258, NGC 4490, NGC 4736, the M 51 group turns at $\kappa = 40$ into an extended association with 405 members, the total K -luminosity of $2.0 \cdot 10^{12}$ and the ratio of the projected mass sum to the sum of group luminosities $\Sigma M_p / \Sigma L_K = 38 M_{\odot}/L_{\odot}$. This loose formation became known in the literature as a Cloud of Galaxies in the Canes Venatici, CVn I.

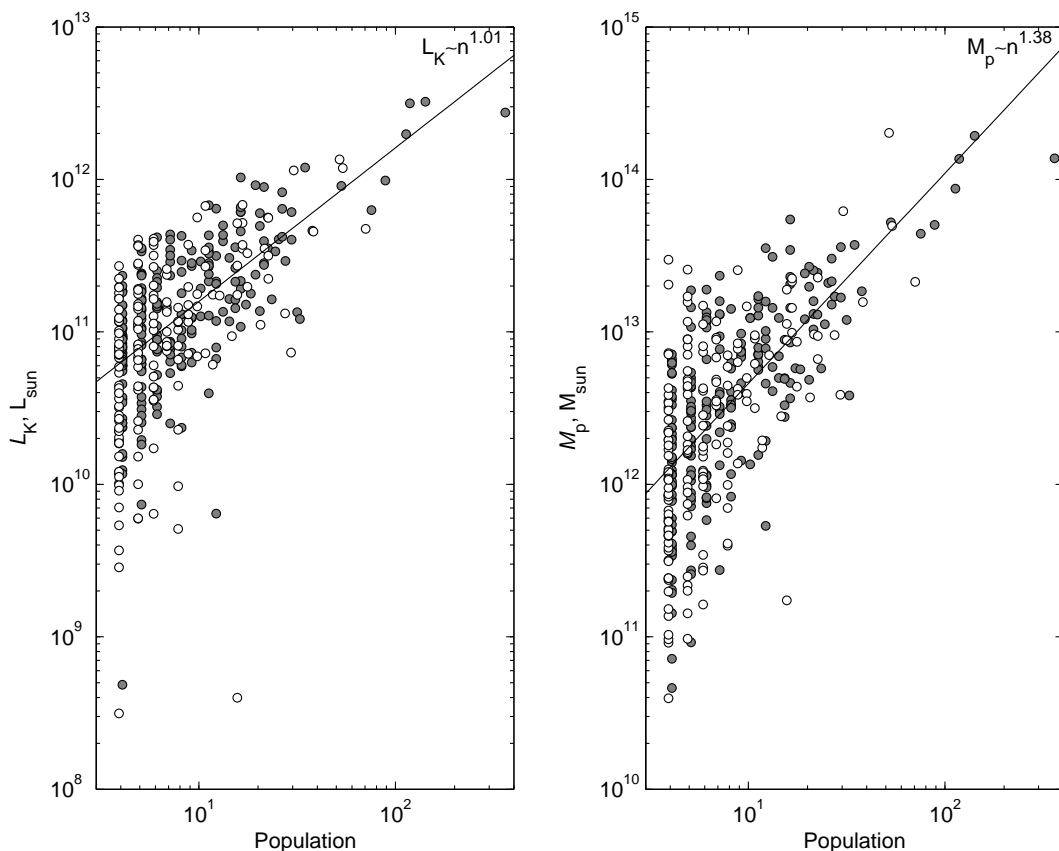


Figure 7. Total K -band luminosity (left panel) and projected mass (right panel) versus the group population with known velocities. The groups with a bulge-dominated principal member are given in grey.

7 BUDGET OF COSMIC MATTER IN THE LOCAL UNIVERSE

The data on galaxies in groups, pairs and in the field available at our disposal allow making judgements on the principal features of the distribution of bright and dark matter in the Local universe with the diameter of 80–90 Mpc. On this scale we expect to reach the mean density of the Universe with accuracy about 15 per cent (Pápai & Szapudi 2010).

Fig. 15 reproduces the distribution of matter in the Local Supercluster and its environs, projected onto the planes {SGX,SGY} and {SGY,SGZ} in the Cartesian supergalactic coordinates. The distance scale is shown by concentric rings around the Local Group with a step of 10 Mpc. The horizontal cones in the left figure are formed by the ‘Zone of Avoidance’ at the galactic latitudes $|b| < 15^\circ$. The Virgo cluster with the adjacent ridges is located up from the centre at a distance of $Y = 17$ Mpc. There is a chain of groups/clusters: Antlia, Hydra, Centaurus seen to the left from Virgo. This structure extends outside the figure’s limits towards the region of the so-called Great Attractor. The Local Void as a zone of low density is seen on the upper side (+Z) of the right panel, adjoining with the cone caused by the Galactic extinction. The surface K -luminosity density in the units of M_\odot/Mpc^2 is shown in grey scale.

Fig. 16 shows the variation of mean density of K -luminosity in the sphere with the radius D_{Mpc} and a step of 1 Mpc. The circles mark the values of the integral luminosity

density of the galaxies belonging to our groups, triplets and pairs. The histogram reflects the course of the mean density with distance for all the galaxies, including the galaxies of the field. The solid, dashed and dotted horizontal lines mark the level of the mean cosmic K -band luminosity density according to Jones et al. (2006); Bell et al. (2003); Cole et al. (2001); Kochanek et al. (2001), who used the 2MASS survey data, but with slightly different assumptions on the proportion of light absorbed by dust inside the galaxies. Within the 40 Mpc radius sphere, the mean density of K -luminosity according to our data amounts to $4.73 \cdot 10^8 L_\odot \text{Mpc}^{-3}$ versus the estimates of the mean space density $(3.8\text{--}4.7) \cdot 10^8 L_\odot \text{Mpc}^{-3}$ from the above sources.

Note that in this volume the total K -luminosity of the galaxies associated into the systems of different multiplicity $n \geq 2$ amounts to 82 per cent of the luminosity of all galaxies. In other words, only 18 per cent of stellar baryons are located outside the boundaries of the virial zones of the galaxy systems. This is in good accordance with luminosity function measurements in groups and overall. For instance, using the data of (Blanton et al. 2003) on total luminosity density and (Zandivarez et al. 2006) on luminosity function in groups from SDSS survey and taking into account the fraction of galaxies in groups (54 per cent), we receive that only 20 per cent of the total light is associated with field galaxies. Comparing the proportion of clustered luminosity in the K -band (82 per cent) with the relative number of clustered galaxies (54 per cent), we conclude that the de-

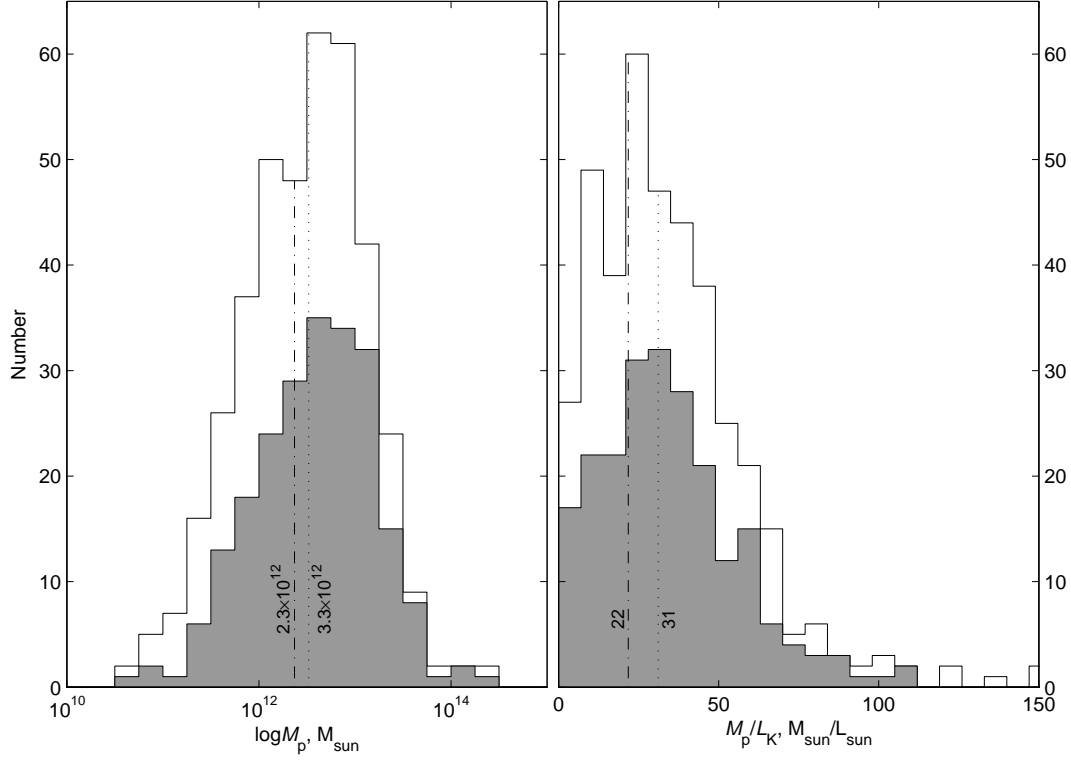


Figure 8. Distribution of the groups by projected mass (left panel) and projected mass-to-K-light ratio (right panel) in the logarithmic scale. The dotted vertical line and the dashed one indicate the biased and unbiased (corrected for velocity measurement errors) medians, respectively.

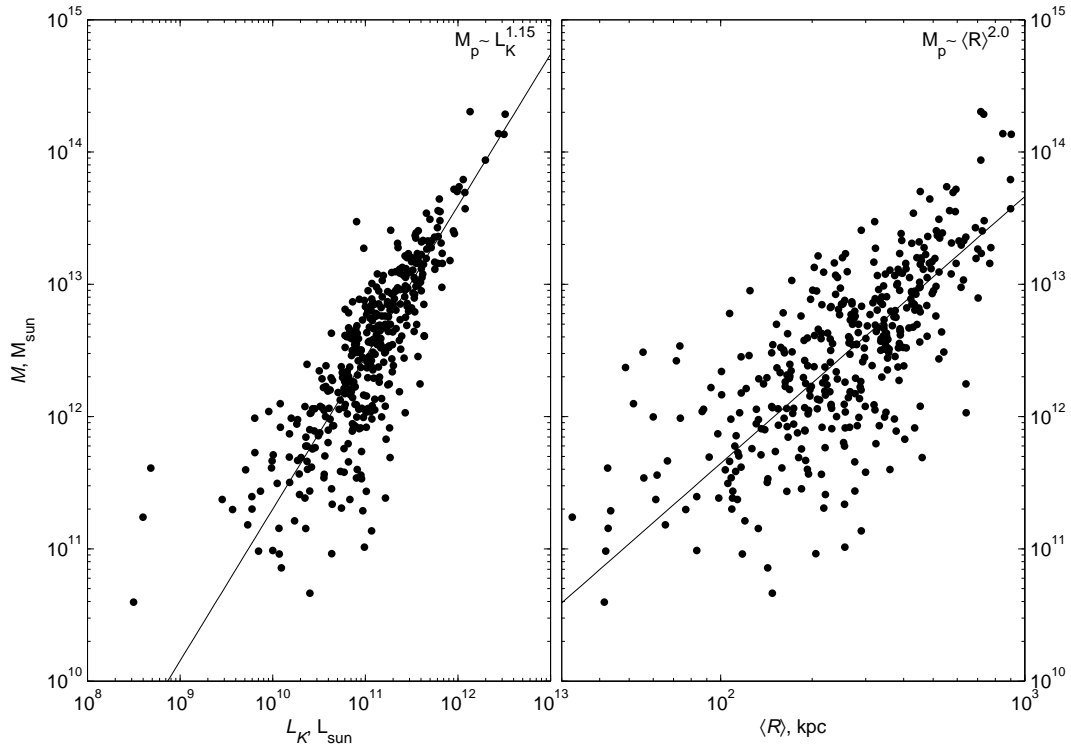


Figure 9. Projected mass of the groups versus their total K -band luminosity (left) and mean projected radius (right panel). The dotted lines show a linear fit to the data.

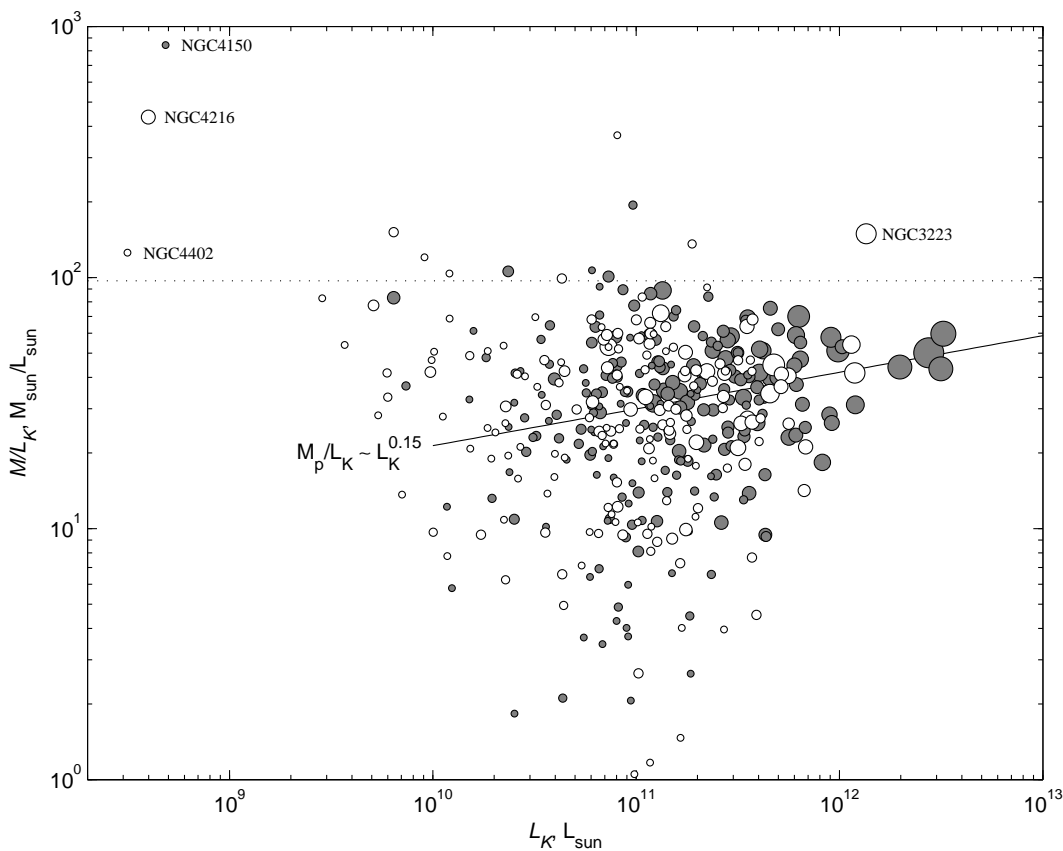


Figure 10. Mass-to-K-light ratio of the groups as a function of K -luminosity. The groups are represented by circles scaled by population. The groups with bulge-dominated main member are shown by filled circles. The horizontal dotted line traces the global cosmic ratio, $97 M_{\odot}/L_{\odot}$, corresponding to $\Omega_m = 0.28$. The regression (solid) line is drawn taking into account the K -luminosity as a statistical weight.

gree of crowding in dwarf galaxies is significantly lower than that in the galaxies with high K -luminosity.

Another feature of the Local universe is revealed in that the approximation of the mean stellar density with increasing D to its asymptotic cosmic value occurs exactly from the top, i.e. the broad LG neighbourhood represents a vast zone of overdensity. At that, the fluctuations $\delta\rho(L_K)/\langle\rho(L_K)\rangle \sim 1$ occur even on the scales of $\sim (15\text{--}20)$ Mpc.

The distribution of mean density of matter in the Local universe is shown in two panels of Fig. 17 in the units of critical density. The contribution of the masses produced by pairs and triplets of galaxies from the catalogues of Karachentsev & Makarov (2008); Makarov & Karachentsev (2009) is shown by the triangles, and the contribution of the masses of groups with a population of $n \geq 4$ is marked by the squares. Apart from the group members, we have to take into account the contribution to the total mass made by the field galaxies. As noted above, their relative number amounts to 46 per cent, and relative luminosity in the K -band is only 18 per cent. We believe that the isolated galaxies differ little in their physical properties from the galaxies in binary or triple systems, as corroborated by the mass estimates from the effects of weak gravitational lensing (Mandelbaum et al. 2006). Attributing to the isolated galaxies the same total mass-luminosity ratios as those possessed by the components of low-multiplicity systems, we have depicted the

behaviour of the total matter density in the volumes of radii D_{Mpc} in the form of a histogram. Compiling the catalogues of groups, triplets and pairs of galaxies, we were limited by the systems, the mean radial velocities of which satisfy the condition $\langle V_{LG} \rangle \leq 3500 \text{ km s}^{-1}$, to which at $H_0 = 73 \text{ km s}^{-1}\text{Mpc}^{-1}$ corresponds the distance of $D = 47.9 \text{ Mpc}$. However, in the process of galaxy clustering we took into account the galaxies beyond this volume with $V_{LG} < 4000 \text{ km s}^{-1}$. Therefore, the values of Ω_m in the $D = 40\text{--}47 \text{ Mpc}$ distance range can be regarded as not highly susceptible to various boundary effects. The histogram in the top panel of Fig. 17 shows that the mean local density of matter within the distance of $40\text{--}47 \text{ Mpc}$ amounts to $\Omega_m = 0.116\text{--}0.096$.

As noted above, the galaxy redshift surveys (CfA, 2dF, 6dF, SDSS) contain a ‘noise’ component $\epsilon_V \simeq 40 \text{ km s}^{-1}$, induced by the velocity measurement errors. It affects the mass estimates in an asymmetric way, overestimating them on the average by 30 per cent. The distribution of the mean density of matter, based on the statistically unbiased estimates of the projected mass is presented in the bottom panel of Fig. 17. The designations here are the same as those on the top panel. In the volumes of radii from 40 to 47 Mpc the mean corrected values of the local density of matter lie in the range of $\Omega_{m,\text{loc}} = 0.092\text{--}0.073$, which is 3–4 times lower than the global cosmological density $\Omega_m = 0.28 \pm 0.03$ in the standard λCDM model (Fukugita & Peebles 2004).

In addition to the galaxy velocity measurement errors,

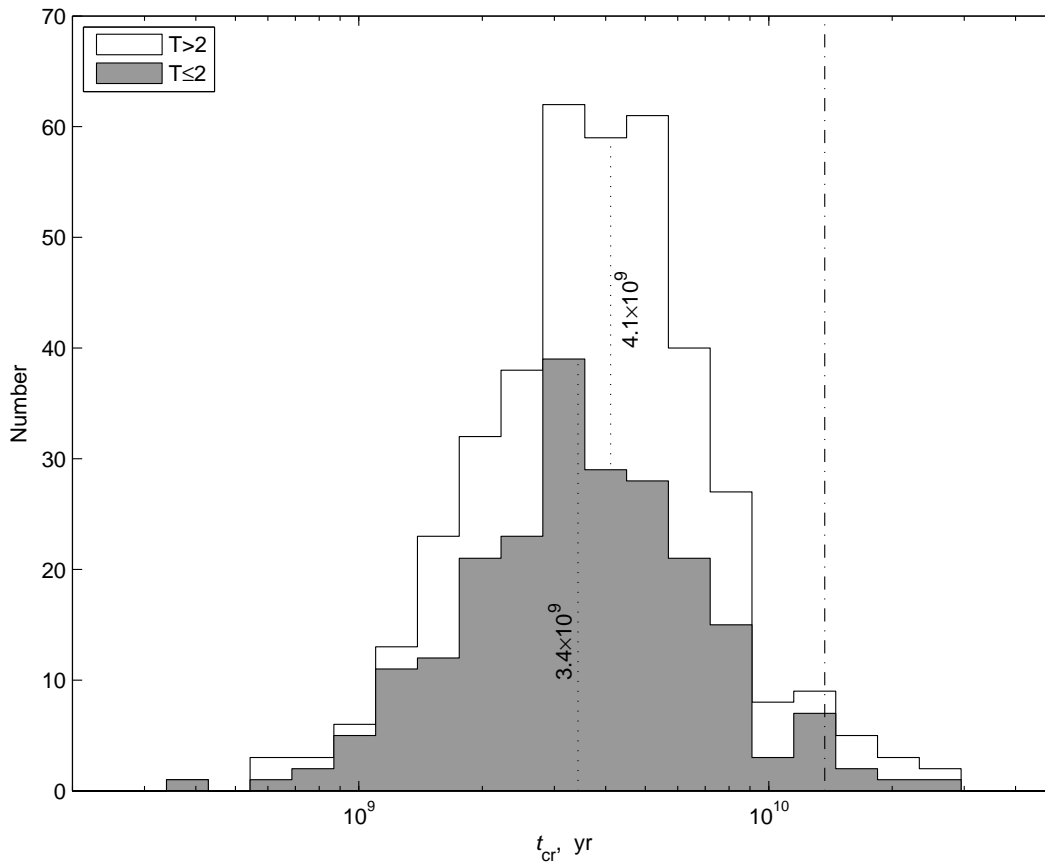


Figure 11. The number of groups with crossing time in the specified intervals. The groups with bulge-dominated principal member are shaded. The vertical line fixes the age of the Universe, 13.7 Gyr.

there is another source of uncertainty in the estimation of the local value of Ω_m . As we have noted, the clustering algorithm we used does not work reliably enough in the regions of large non-Hubble motions. Summing the mass of groups we identified in the Virgo cluster volume ($6.0 \cdot 10^{14} M_\odot$), we found that it was smaller than the virial mass estimate $7.0 \cdot 10^{14} M_\odot$. In the case of the Fornax cluster, the total mass of the groups turned out to be larger than the virial mass ($2.1 \cdot 10^{14} M_\odot$ versus $0.6 \cdot 10^{14} M_\odot$). Therefore, at the total mass of the local sphere with the radius of 40 Mpc equal to $(2.7\text{--}3.4) \cdot 10^{15} M_\odot$, the errors of mass determination $\sim 2 \cdot 10^{14} M_\odot$ result in the error in the Ω_m estimations of less than 10 per cent.

Another reason, distorting the local estimate of Ω_m , can be the fact that we neglected the galaxies that do not yet have their radial velocities measured. In order to determine the significance of their contribution, we assumed that the luminosity function of galaxies is described by the Schechter (1976) function with the parameters $M_K^* = -24.3$ and $\alpha = -1.0$ (Bell et al. 2003; Cole et al. 2001). In the galaxy redshift surveys (6dF, SDSS) the completeness of radial velocity measurements is assured up to the limiting apparent magnitude $K_s \simeq 12.0^m$. At the boundary of the volume under consideration (40–47) Mpc, this corresponds to the absolute magnitude of (-21.0) , by 3^m fainter than M_K^* . With the above parameters of the luminosity function, the contribution of the fainter galaxies in the integral luminosity on the edge of the considered volume is only about

12 per cent. In general, the correction to the mean luminosity density over the entire volume is less than 10 per cent. Consequently, the neglect of galaxies without measured radial velocities, and an imperfection of the group criterion we used may not be the causes of such a strong difference in the estimates of local and global densities of matter.

8 CONCLUDING REMARKS

The main objective of our work was to create a catalogue of galaxy groups, covering the entire sky and extending up to the distances of 40–45 Mpc from the Local Group. To this end, we used the clustering algorithm that takes into account individual characteristics of galaxies. Applying this criterion to the observational data on 10914 galaxies with the velocities $V_{LG} < 3500 \text{ km s}^{-1}$, we have identified 509 pairs, 168 triple systems and 395 groups with the populations of four or more members. Totally these samples include 54 per cent of all galaxies, or 82 per cent of the total luminosity of the Local universe of the given volume. At that, we have not used any special conditions that would restrict the initial sample of galaxies by morphological type or other characteristics (apart from the availability of radial velocity measurements). Minimal selectivity of our sample makes it attractive for the analysis of various properties of galaxy systems depending on their environment.

We consider that the most important result here is

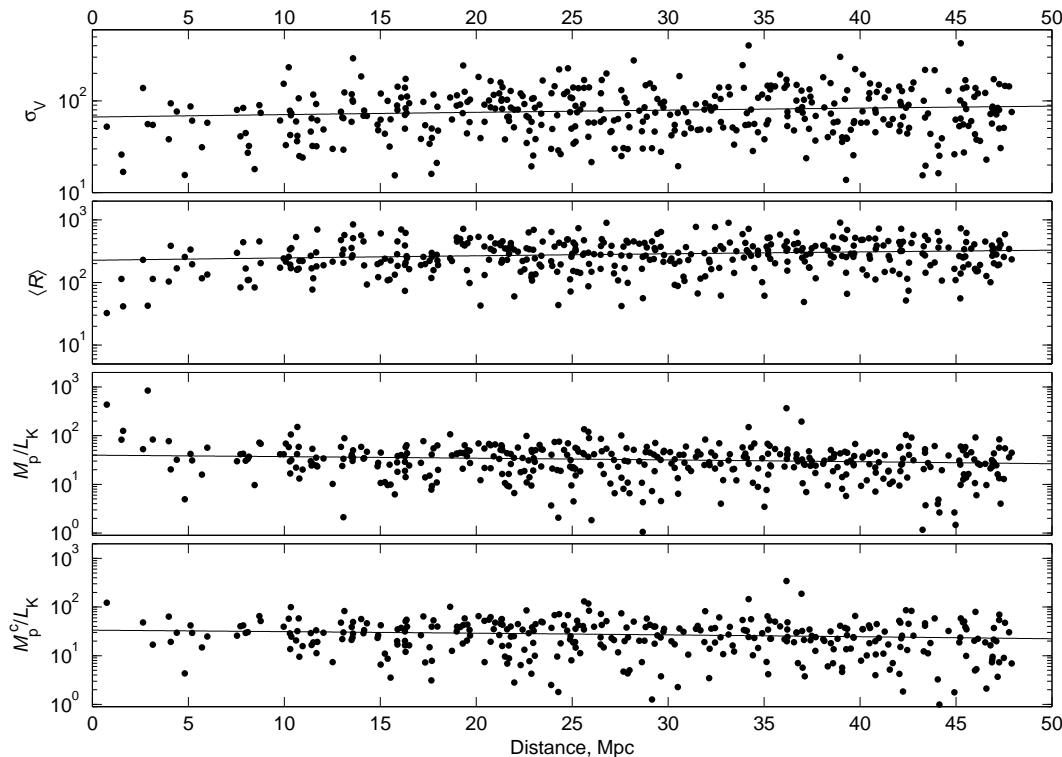


Figure 12. From top to bottom: velocity dispersion, mean projected radius, projected mass-to-light ratio and corrected mass-to-light ratio as a function of distance. The solid lines show a linear fit to the data.

the estimation of the mean density of matter in the Local universe. According to our data, its value amounts to $\Omega_m = 0.08 \pm 0.02$ in the spherical volume with the diameter of 80–90 Mpc. As noted above, the low estimates of $\Omega_m \sim 0.10$ also follow from the virial masses in galaxy groups derived from the lists by Vennik (1984); Tully (1988); Magtesyan (1988). In a recent paper by Crook et al. (2007) the estimates of Ω_m were obtained ranging from 0.10 to 0.23, depending on the choice of parameters for galaxy association into groups, and on the way of computing the virial masses of groups. Earlier, Bahcall et al. (2000) studied the published estimates of the mass-luminosity ratio in the groups and clusters, and deduced the value $\Omega_m = 0.16 \pm 0.05$. Recently, Abate & Erdoğan (2009) analysed the peculiar velocity field for the 2MASS galaxies, using the SFI++ survey data (Springob et al. 2007), and concluded that in the Local universe with a characteristic scale of $\sim 6000 \text{ km s}^{-1}$ the density of matter lies within the interval of $\Omega_m = 0.09\text{--}0.23$.

At least, three different ideas can be proposed to explain the drastic difference between the local and the global estimates of Ω_m .

(i) Dark matter in groups and clusters extends far beyond their virial radius traced by galaxies. To reduce the Ω_m discrepancy, one ought to assume that the total mass of each group and cluster is about 3 times its virial mass. However, as it was shown by Karachentsev (2005); Karachentsev & Nasonova (2010); Nasonova et al. (2011), the total mass of nearby groups and Virgo, Fornax clusters within the radius of zero velocity surface R_0 is almost the same as their virial mass. Note that R_0 is $\sim (3.5\text{--}4.0)R_{\text{vir}}$. Therefore, the exis-

tence of large amount of dark matter at periphery of systems is inconsistent with the observational data.

(ii) One can imagine a possibility that the local Universe is significantly (3 times) under-dense relative to the global density. The largest structure in the Universe detected to date is the Sloan Great Wall, filamentary aggregation of galaxies of 450 Mpc long, at distance of 310 Mpc (Gott et al. 2005). In principle, we can reside in a “valley” between such kind large scale walls. But, Fig. 16 tells us that we are living in the luminous matter overdensity extending till to about 40 Mpc. Of course, this local overdensity can be only a peak surrounded by wider under-dense region. However, numerous K -band counts of galaxies in the range of $K = 12\text{--}19^m$ (Djorgovski et al. 1995; Bershadsky et al. 1998; Huang et al. 2001; Totani et al. 2001) do not show the presence of any significant cosmic lacuna around us within ~ 2000 Mpc.

(iii) It is possible that essential part of dark matter in the Universe (about 2/3) is scattered outside virial (and even collapsing) regions being concentrated in dark clumps or distributed as a homogeneous dark “sea”. Some observational arguments favourable to the existence of massive dark clumps have been presented by Natarajan & Springel (2004); Jee et al. (2005) from weak lensing, and by Karachentsev et al. (2006) from properties of disturbed isolated galaxies.

ACKNOWLEDGMENTS

The authors are grateful to V.E. Karachentseva for the great work on the verification and refinement of the original observational data. We are thankful to Brent Tully, Stefan Gottlöber and Helene Courtois for discussions and

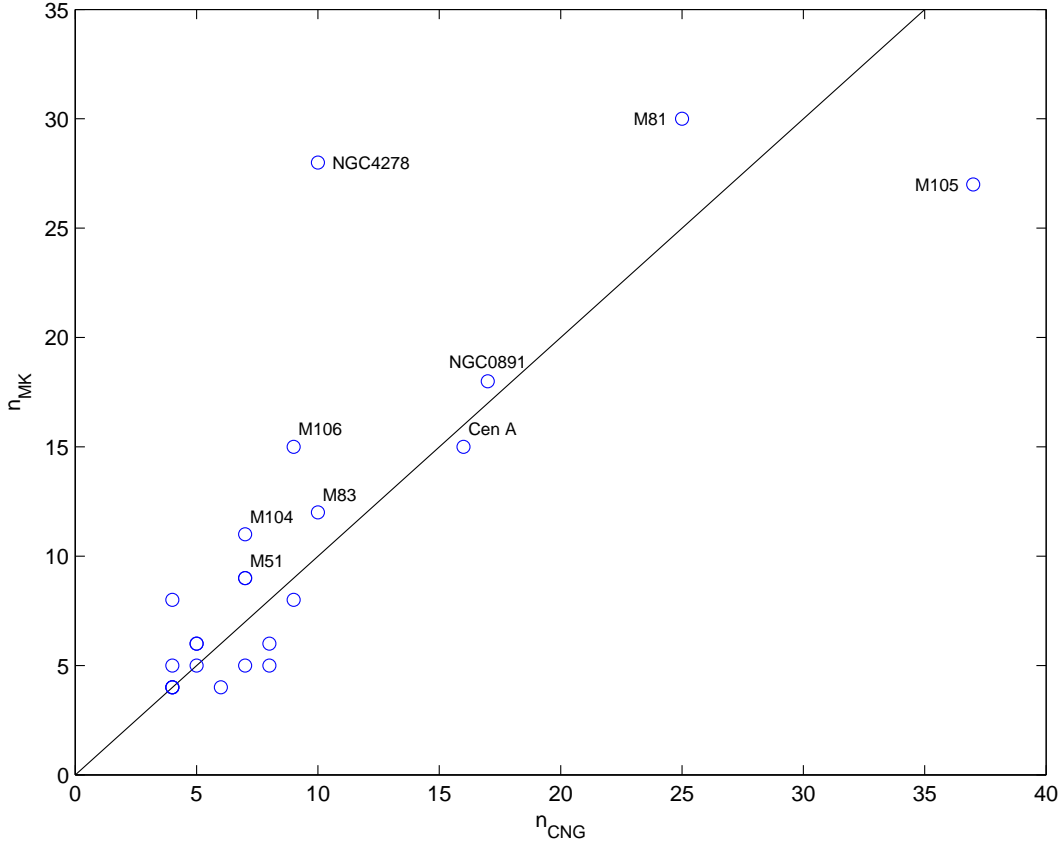


Figure 13. Number of galaxies in the Local Volume groups (with known velocities) identified by the clustering algorithm versus their number in the same groups as presented in CNG-catalogue (Karachentsev et al. 2004).

useful comments. We acknowledge the usage of the HyperLEDA database³. This research has made use of the NASA/IPAC Extragalactic Database⁴ which is operated by the Jet Propulsion Laboratory, California Institute of Technology, under contract with the National Aeronautics and Space Administration. We acknowledge the usage of the HIPASS public data release⁵. This work was supported by the RFBR grants 10-02-00123, 08-02-00627, RUS-UKR 09-02-90414.

REFERENCES

- Abate A., Erdoğan P., 2009, *MNRAS*, 400, 1541
 Abazajian K. N., Adelman-McCarthy J. K., Agüeros M. A., Allam S. S., Allende Prieto C., An D., Anderson K. S. J., Anderson S. F., Annis J., Bahcall N. A., Bailer-Jones C. A. L., Barentine J. C., Bassett B. A., Becker A. C., Beers T. C., Bell E. F., Belokurov V., Berlind A. A., Berman E. F., Bernardi M., Bickerton S. J., Bizyaev D., Blakeslee J. P., Blanton M. R., Bochanski J. J., Boroski W. N., Brewington H. J., Brinchmann J., Brinkmann J., Brunner R. J., Budavári T., Carey L. N., Carliles S., Carr M. A., Castander F. J., Cinabro D., Connolly A. J., Csabai I., Cunha C. E., Czarapata P. C., Davenport J. R. A., de Haas E., Dilday B., Doi M., Eisenstein D. J., Evans M. L., Evans N. W., Fan X., Friedman S. D., Frieman J. A., Fukugita M., Gänsicke B. T., Gates E., Gillespie B., Gilmore G., Gonzalez B., Gonzalez C. F., Grebel E. K., Gunn J. E., Györy Z., Hall P. B., Harding P., Harris F. H., Harvanek M., Hawley S. L., Hayes J. J. E., Heckman T. M., Hendry J. S., Hennessy G. S., Hindsley R. B., Hoblitt J., Hogan C. J., Hogg D. W., Holtzman J. A., Hyde J. B., Ichikawa S., Ichikawa T., Im M., Ivezić Ž., Jester S., Jiang L., Johnson J. A., Jorgensen A. M., Jurić M., Kent S. M., Kessler R., Kleinman S. J., Knapp G. R., Konishi K., Kron R. G., Krzesinski J., Kuropatkin N., Lampeitl H., Lebedeva S., Lee M. G., Lee Y. S., Leger R. F., Lépine S., Li N., Lima M., Lin H., Long D. C., Loomis C. P., Loveday J., Lupton R. H., Magnier E., Malanushenko O., Malanushenko V., Mandelbaum R., Margon B., Marriner J. P., Martínez-Delgado D., Matsubara T., McGehee P. M., McKay T. A., Meiksin A., Morrison H. L., Mullally F., Munn J. A., Murphy T., Nash T., Nebot A., Neilsen E. H., Newberg H. J., Newman P. R., Nichol R. C., Nicinski T., Nieto-Santisteban M., Nitta A., Okamura S., Oravetz D. J., Ostriker J. P., Owen R., Padmanabhan N., Pan K., Park C., Pauls G., Peoples J., Percival W. J., Pier J. R., Pope A. C., Pourbaix D., Price P. A., Purger N., Quinn T., Raddick M. J., Fiorentin P. R., Richards G. T., Richmond M. W., Riess A. G., Rix H., Rockosi C. M., Sako M., Schlegel D. J.,

³ <http://leda.univ-lyon1.fr>

⁴ <http://nedwww.ipac.caltech.edu/>

⁵ <http://www.atnf.csiro.au/research/multibeam/release/>

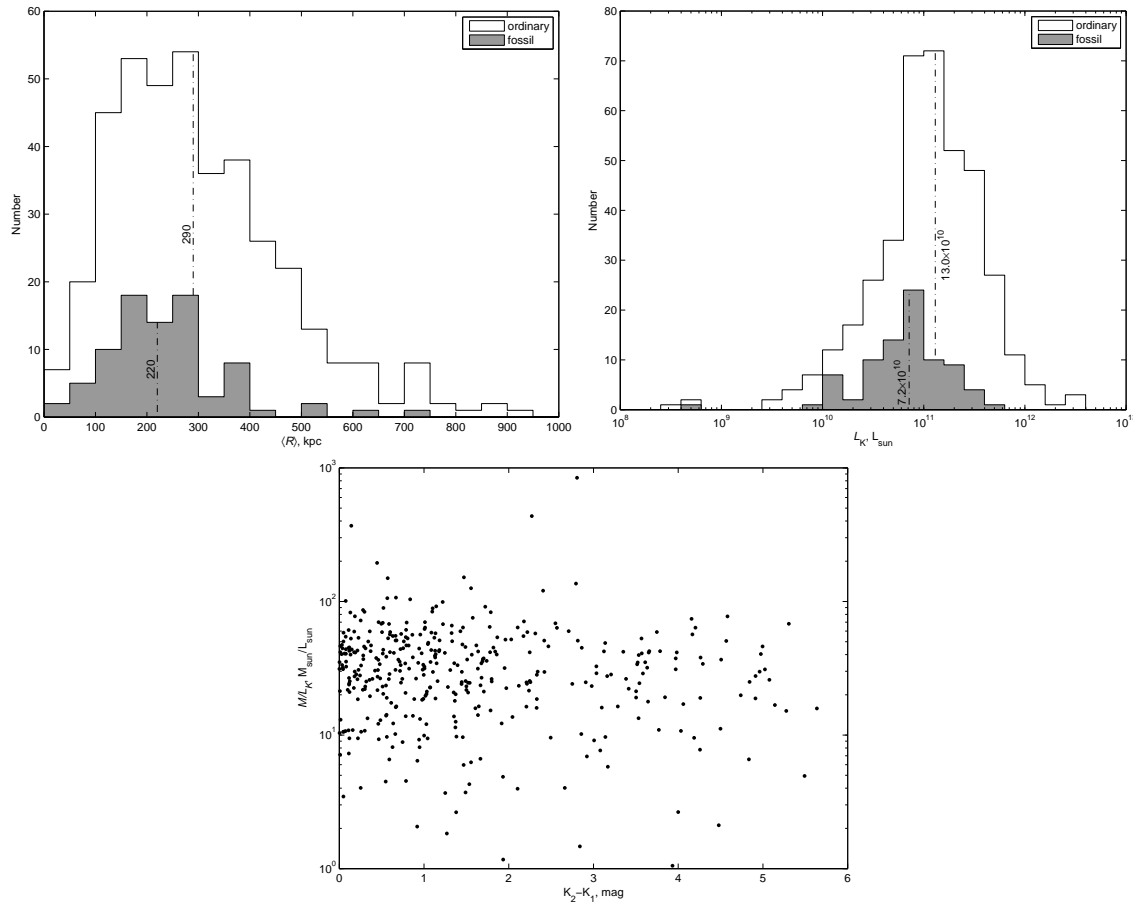


Figure 14. Properties of ‘fossil’ groups (shaded) with respect to others. Top left: number of groups versus mean projected radius. Top right: number of groups versus K -luminosity. Bottom: projected mass-to-luminosity ratio as a function of K -magnitude difference between the first and the second ranked members.

Figure 15. Distribution of matter projected onto the supergalactic planes SGX, SGY and SGZ. The distance scale is given by concentric rings around the Local Group with a step of 10 Mpc.

Schneider D. P., Scholz R., Schreiber M. R., Schwöpe A. D., Seljak U., Sesar B., Sheldon E., Shimasaku K., Sibley V. C., Simmons A. E., Sivarani T., Smith J. A., Smith M. C., Smolčić V., Snedden S. A., Stebbins A., Steinmetz M., Stoughton C., Strauss M. A., Subba Rao M., Suto Y., Szalay A. S., Szapudi I., Szkody P., Tanaka M., Tegmark M., Teodoro L. F. A., Thakar A. R., Tremonti C. A., Tucker D. L., Uomoto A., Vanden Berk D. E., Vandenberg J., Vidrih S., Vogeley M. S., Voges W., Vogt N. P., Wadadekar Y., Watters S., Weinberg D. H., West A. A., White S. D. M., Wilhite B. C., Wonders A. C., Yanny B., Yocum D. R., York D. G., Zehavi I., Zibetti S., Zucker D. B., 2009, *ApJS*, 182, 543

Bahcall N. A., Cen R., Davé R., Ostriker J. P., Yu Q., 2000, *ApJ*, 541, 1

Barnes D. G., Staveley-Smith L., de Blok W. J. G., Oosterloo T., Stewart I. M., Wright A. E., Banks G. D., Bhattacharjee R., Boyce P. J., Calabretta M. R., Disney M. J., Drinkwater M. J., Ekers R. D., Freeman K. C., Gibson B. K., Green A. J., Haynes R. F., de Lint H., Hekker P., Henning P. A., Jerjen H., Juraszek S., Kesteven M. J., Kilborn V. A., Knezek P. M., Koribalski B., Kraan-Korteweg

R. C., Malin D. F., Marquarding M., Minchin R. F., Mould J. R., Price R. M., Putman M. E., Ryder S. D., Sadler E. M., Schröder A., Stootman F., Webster R. L., Wilson W. E., Ye T., 2001, *MNRAS*, 322, 486

Bell E. F., McIntosh D. H., Katz N., Weinberg M. D., 2003, *ApJS*, 149, 289

Bershady M. A., Lowenthal J. D., Koo D. C., 1998, *ApJ*, 505, 50

Binggeli B., Sandage A., Tammann G. A., 1985, *AJ*, 90, 1681

Binney J., Merrifield M., 1998, *Galactic astronomy*, Binney, J. & Merrifield, M., ed.

Blanton M. R., Hogg D. W., Bahcall N. A., Brinkmann J., Britton M., Connolly A. J., Csabai I., Fukugita M., Loveday J., Meiksin A., Munn J. A., Nichol R. C., Okamura S., Quinn T., Schneider D. P., Shimasaku K., Strauss M. A., Tegmark M., Vogeley M. S., Weinberg D. H., 2003, *ApJ*, 592, 819

Buzzoni A., 2005, *MNRAS*, 361, 725

Cole S., Norberg P., Baugh C. M., Frenk C. S., Bland-Hawthorn J., Bridges T., Cannon R., Colless M., Collins C., Couch W., Cross N., Dalton G., De Propris R., Driver

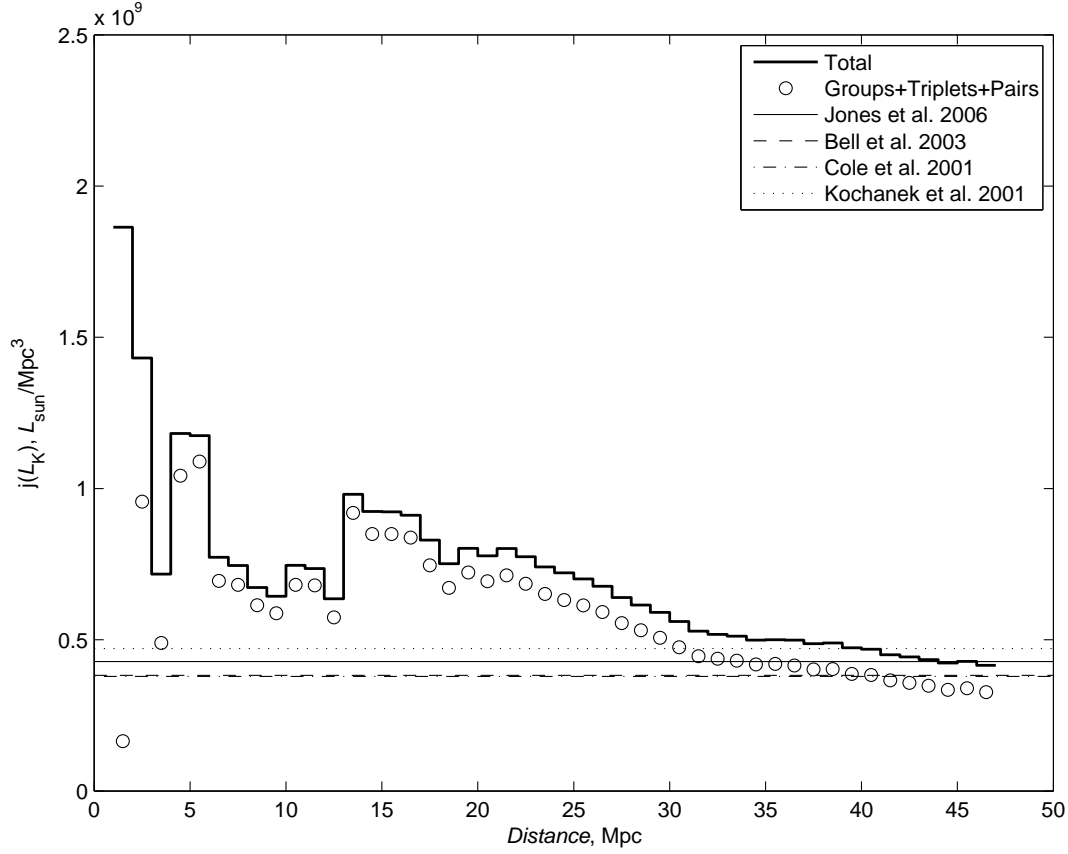


Figure 16. The mean K -band luminosity density as a function of distance. The density for the groups, triplets and pairs is shown by circles, and the total density including field galaxies is plotted by histogram. Three horizontal lines represent asymptotic K -band luminosity density from 2MASS by different authors.

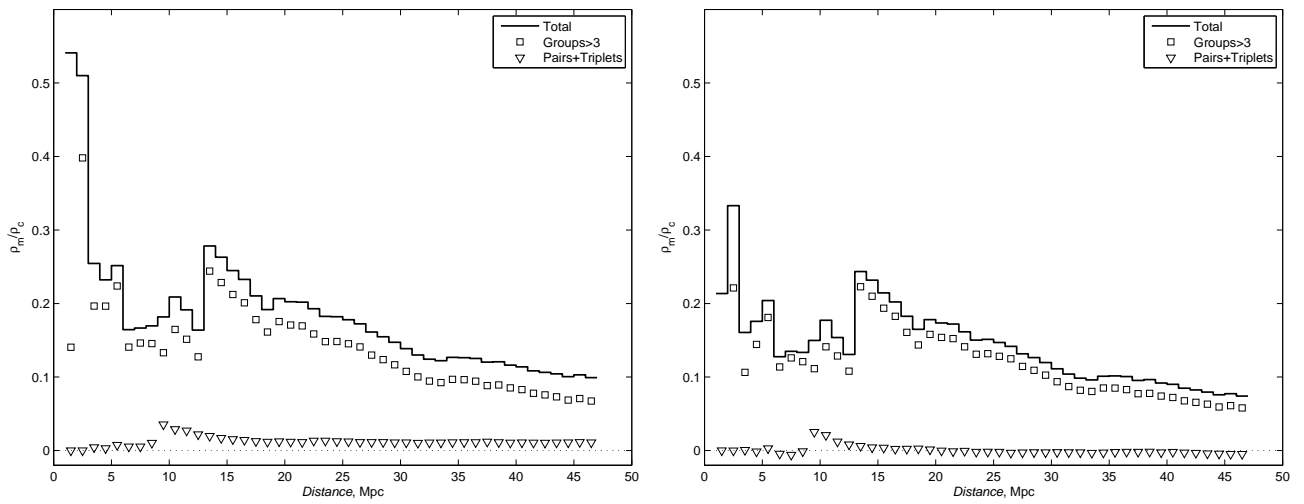


Figure 17. The mean density of matter as a function of distance. Contributions of groups and pairs + triplets are shown by squares and triangles, respectively. The total mass density is plotted by histogram. Left: biased mass estimates ignoring radial velocity errors. Right: unbiased matter density corrected for the velocity errors.

- S. P., Efstathiou G., Ellis R. S., Glazebrook K., Jackson C., Lahav O., Lewis I., Lumsden S., Maddox S., Madgwick D., Peacock J. A., Peterson B. A., Sutherland W., Taylor K., 2001, *MNRAS*, 326, 255
- Colless M., Dalton G., Maddox S., Sutherland W., Norberg P., Cole S., Bland-Hawthorn J., Bridges T., Cannon R., Collins C., Couch W., Cross N., Deeley K., De Propriis R., Driver S. P., Efstathiou G., Ellis R. S., Frenk C. S., Glazebrook K., Jackson C., Lahav O., Lewis I., Lumsden S., Madgwick D., Peacock J. A., Peterson B. A., Price I., Seaborne M., Taylor K., 2001, *MNRAS*, 328, 1039
- Crook A. C., Huchra J. P., Martimbeau N., Masters K. L., Jarrett T., Macri L. M., 2007, *ApJ*, 655, 790
- de Vaucouleurs G., de Vaucouleurs A., Corwin J. R., 1976, in *Second reference catalogue of bright galaxies*, 1976, Austin: University of Texas Press., pp. 0–+
- Desai V., Dalcanton J. J., Mayer L., Reed D., Quinn T., Governato F., 2004, *MNRAS*, 351, 265
- Díaz-Giménez E., Muriel H., Mendes de Oliveira C., 2008, *A&A*, 490, 965
- Djorgovski S., Soifer B. T., Pahre M. A., Larkin J. E., Smith J. D., Neugebauer G., Smail I., Matthews K., Hogg D. W., Blandford R. D., Cohen J., Harrison W., Nelson J., 1995, *ApJ*, 438, L13
- Eigenthaler P., Zeilinger W. W., 2010, *A&A*, 511, A12+
- Ferguson H. C., 1989, *AJ*, 98, 367
- Ferguson H. C., Sandage A., 1990, *AJ*, 100, 1
- Fukugita M., Peebles P. J. E., 2004, *ApJ*, 616, 643
- Fukugita M., Shimasaku K., Ichikawa T., 1995, *PASP*, 107, 945
- Giovanelli R., Haynes M. P., Kent B. R., Perillat P., Saintonge A., Brosch N., Catinella B., Hoffman G. L., Stierwalt S., Spekkens K., Lerner M. S., Masters K. L., Momjian E., Rosenberg J. L., Springob C. M., Boselli A., Charmandaris V., Darling J. K., Davies J., Garcia Lambas D., Gavazzi G., Giovanardi C., Hardy E., Hunt L. K., Iovino A., Karachentsev I. D., Karachentseva V. E., Koopmann R. A., Marinoni C., Minchin R., Muller E., Putman M., Pantoja C., Salzer J. J., Scodreggio M., Skillman E., Solanes J. M., Valotto C., van Driel W., van Zee L., 2005, *AJ*, 130, 2598
- Gott III J. R., Jurić M., Schlegel D., Hoyle F., Vogeley M., Tegmark M., Bahcall N., Brinkmann J., 2005, *ApJ*, 624, 463
- Heisler J., Tremaine S., Bahcall J. N., 1985, *ApJ*, 298, 8
- Hoffman G. L., Olson D. W., Salpeter E. E., 1980, *ApJ*, 242, 861
- Huang J., Thompson D., Kümmel M. W., Meisenheimer K., Wolf C., Beckwith S. V. W., Fockenbrock R., Fried J. W., Hippelein H., von Kuhlmann B., Phleps S., Röser H., Thommes E., 2001, *A&A*, 368, 787
- Huchra J. P., Geller M. J., 1982, *ApJ*, 257, 423
- Jarrett T. H., Chester T., Cutri R., Schneider S., Skrutskie M., Huchra J. P., 2000, *AJ*, 119, 2498
- Jarrett T. H., Chester T., Cutri R., Schneider S. E., Huchra J. P., 2003, *AJ*, 125, 525
- Jee M. J., White R. L., Benítez N., Ford H. C., Blakeslee J. P., Rosati P., Demarco R., Illingworth G. D., 2005, *ApJ*, 618, 46
- Jones D. H., Peterson B. A., Colless M., Saunders W., 2006, *MNRAS*, 369, 25
- Jones D. H., Saunders W., Colless M., Read M. A., Parker Q. A., Watson F. G., Campbell L. A., Burkey D., Mauch T., Moore L., Hartley M., Cass P., James D., Russell K., Fiegert K., Dawe J., Huchra J., Jarrett T., Lahav O., Lucey J., Mamon G. A., Proust D., Sadler E. M., Wakamatsu K., 2004, *MNRAS*, 355, 747
- Jones L. R., Ponman T. J., Horton A., Babul A., Ebeling H., Burke D. J., 2003, *MNRAS*, 343, 627
- Karachentsev I., 1994, *Astronomical and Astrophysical Transactions*, 6, 1
- Karachentsev I. D., 2005, *AJ*, 129, 178
- Karachentsev I. D., Karachentseva V. E., 2004, *Astronomy Reports*, 48, 267
- Karachentsev I. D., Karachentseva V. E., Huchtmeier W. K., 2006, *A&A*, 451, 817
- , 2007, *Astronomy Letters*, 33, 512
- Karachentsev I. D., Karachentseva V. E., Huchtmeier W. K., Makarov D. I., 2004, *AJ*, 127, 2031
- Karachentsev I. D., Kutkin A. M., 2005, *Astronomy Letters*, 31, 299
- Karachentsev I. D., Makarov D. I., 2008, *Astrophysical Bulletin*, 63, 299
- Karachentsev I. D., Makarov D. I., Karachentseva V. E., Melnik O. V., 2008, *Astronomy Letters*, 34, 832
- Karachentsev I. D., Makarov D. I., Karachentseva V. E., Melnyk O. V., 2009, *ArXiv e-prints*
- Karachentsev I. D., Nasonova O. G., 2010, *MNRAS*, 405, 1075
- Karachentseva V. E., Karachentsev I. D., 1998, *A&AS*, 127, 409
- , 2000, *A&AS*, 146, 359
- Karachentseva V. E., Melnyk O. V., Karachentsev I. D., Makarov D. I., 2011, in preparation
- Kochanek C. S., Pahre M. A., Falco E. E., Huchra J. P., Mader J., Jarrett T. H., Chester T., Cutri R., Schneider S. E., 2001, *ApJ*, 560, 566
- Magtesyan A. P., 1988, *Astrophysics*, 28, 150
- Mahdavi A., Trentham N., Tully R. B., 2005, *AJ*, 130, 1502
- Maia M. A. G., da Costa L. N., Latham D. W., 1989, *ApJS*, 69, 809
- Makarov D. I., Karachentsev I. D., 2000, in *Astronomical Society of the Pacific Conference Series*, Vol. 209, IAU Colloq. 174: Small Galaxy Groups, M. J. Valtonen & C. Flynn, ed., pp. 40–+
- , 2009, *Astrophysical Bulletin*, 64, 24
- Mandelbaum R., Seljak U., Kauffmann G., Hirata C. M., Brinkmann J., 2006, *MNRAS*, 368, 715
- Materne J., 1978, *A&A*, 63, 401
- , 1979, *A&A*, 74, 235
- McLaughlin D. E., 1999, *ApJ*, 512, L9
- Mieske S., Hilker M., Infante L., Mendes de Oliveira C., 2007, *A&A*, 463, 503
- Nasonova O. G., Peirani S., de Freitas Pacheco J. A., 2011, in preparation
- Natarajan P., Springel V., 2004, *ApJ*, 617, L13
- Pápai P., Szapudi I., 2010, *ArXiv e-prints*
- Paturel G., Petit C., Prugniel P., Theureau G., Rousseau J., Brouty M., Dubois P., Cambrésy L., 2003, *A&A*, 412, 45
- Sandage A., 1986, *ApJ*, 307, 1
- Schechter P., 1976, *ApJ*, 203, 297
- Schlegel D. J., Finkbeiner D. P., Davis M., 1998, *ApJ*, 500, 525

- Spergel D. N., Bean R., Doré O., Nolta M. R., Bennett C. L., Dunkley J., Hinshaw G., Jarosik N., Komatsu E., Page L., Peiris H. V., Verde L., Halpern M., Hill R. S., Kogut A., Limon M., Meyer S. S., Odegard N., Tucker G. S., Weiland J. L., Wollack E., Wright E. L., 2007, *ApJS*, 170, 377
- Springob C. M., Masters K. L., Haynes M. P., Giovanelli R., Marinoni C., 2007, *ApJS*, 172, 599
- Tonry J. L., Blakeslee J. P., Ajhar E. A., Dressler A., 2000, *ApJ*, 530, 625
- Tonry J. L., Dressler A., Blakeslee J. P., Ajhar E. A., Fletcher A. B., Luppino G. A., Metzger M. R., Moore C. B., 2001, *ApJ*, 546, 681
- Totani T., Yoshii Y., Maihara T., Iwamuro F., Motohara K., 2001, *ApJ*, 559, 592
- Trentham N., Tully R. B., 2009, *MNRAS*, 398, 722
- Tully R. B., 1987, *ApJ*, 321, 280
- , 1988, *Nearby galaxies catalog*, Tully, R. B., ed.
- Tully R. B., Fisher J. R., 1977, *A&A*, 54, 661
- Tully R. B., Shaya E. J., 1984, *ApJ*, 281, 31
- Tully R. B., Trentham N., 2008, *AJ*, 135, 1488
- Vennik J., 1984, *Tartu Astrofüüsika Observatoorium Teated*, 73, 1
- , 1987, *Dissertation*. Tartu
- von Benda-Beckmann A. M., D’Onghia E., Gottlöber S., Hoefl M., Khalatyan A., Klypin A., Müller V., 2008, *MNRAS*, 386, 2345
- Zandivarez A., Martínez H. J., Merchán M. E., 2006, *ApJ*, 650, 137

This figure "ass1200.png" is available in "png" format from:

<http://arxiv.org/ps/1011.6277v1>

This figure "sky1200.png" is available in "png" format from:

<http://arxiv.org/ps/1011.6277v1>

This figure "ass2400.png" is available in "png" format from:

<http://arxiv.org/ps/1011.6277v1>

This figure "sky2400.png" is available in "png" format from:

<http://arxiv.org/ps/1011.6277v1>

This figure "ass3500.png" is available in "png" format from:

<http://arxiv.org/ps/1011.6277v1>

This figure "sky3500.png" is available in "png" format from:

<http://arxiv.org/ps/1011.6277v1>

This figure "xyldens.png" is available in "png" format from:

<http://arxiv.org/ps/1011.6277v1>

This figure "yzldens.png" is available in "png" format from:

<http://arxiv.org/ps/1011.6277v1>